OPTICAL HARMONIC GENERATION PARAMETRIC DEVICES

The scope of this article is mainly focused on optical harmonic generators and parametric generators. These devices are based on nonlinear optical interactions to generate or amplify one or several laser beams. They offer a unique opportunity to achieve an optical frequency conversion; furthermore, their conversion efficiency may reach 85% for the best performing ones. Nowadays, most of these systems use 3-wave interactions in noncentrosymmetric and anisotropic crystals. These interactions consist of sum and difference frequency mixing, SFM and DFM, respectively, as shown in Fig. 1. Harmonic generations are particular cases of SFM. This introduction begins with a rapid overview of nonlinear optics in order to present the main issues closely related to that of parametric devices. The main applications of these systems will then be presented.

NONLINEAR OPTICS: AN ACTUAL AND WIDE FIELD OF OPTICS RESEARCH

Since the first observation of second harmonic generation by Franken in 1961, the field of nonlinear optics (NLO) has become extremely diverse, with a still increasing variety of applications. The wide range of phenomena gathered under the index term *nonlinear optics* were described for their main parts in the 1960s, together with the related theoretical background. The reader may usefully refer to specialized books such as those cited in Refs. (1) and (2). However, the number of papers, conferences, and patents relating to NLO is still increasing nowadays, mainly because of the numerous potential applications of optoelectronic devices. Furthermore, since 1960 these studies have benefited from constant progress on both laser sources and optical materials.

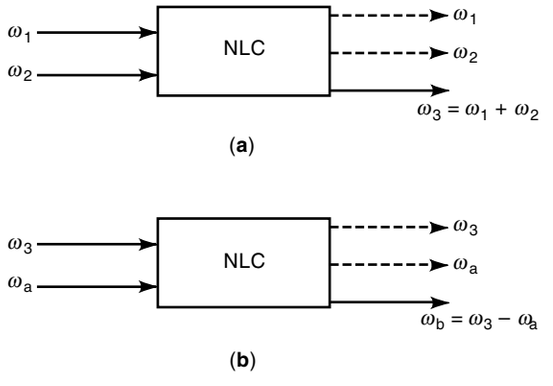

Figure 1. 3-wave interaction in a noncentrosymmetric nonlinear crystal (NLC): (a) sum frequency mixing $\omega_3 = \omega_1 + \omega_2$, second harmonic generation (SHG) $2\omega = \omega + \omega$, third harmonic generation (THG) $3\omega = 2\omega + \omega$; (b) difference frequency mixing (DFM) $\omega_b = \omega_3 - \omega_a$ with $(\omega_a, \omega_b) = (\omega_1, \omega_2)$ or (ω_2, ω_1).

Nonlinear optical phenomena are analogous effects, such as harmonic generation, parametric amplification, and rectification, which are well-known to electrical engineers at audio, radio, and microwave frequencies. All of these have their counterpart at optical frequencies, between 10^{13} Hz and 10^{15} Hz, corresponding to ultraviolet, visible, near, and mid infrared spectra. This is a consequence of the nonlinear response of a medium to an applied optical field.

In terms of linear optics, developed for centuries, the propagation of an electromagnetic wave in a dielectric medium is schematically described as follows: the optical field at circular frequency ω creates dipoles by displacing the valence electrons of all the different atoms of the material (the motion of the heavy nuclei is generally neglected at the considered frequencies); this induces a macroscopic electronic polarization, which in return radiates a field proportional to the incident one and with the same vibration ω. The associated refractive index n is a rank two tensor, characteristic of the medium; it is symptomatic of the structural arrangement of the atoms in the medium. Under these conditions, two waves at different frequencies cannot interact.

The consideration of a linear response of the medium is only an approximation, which is currently done in many domains of physics. If the amplitude of the incoming electric fields is large, the induced polarization is nonlinear with respect to those fields, and waves can interact together. In such a case, the motion of the electrons becomes anharmonic and so the dipoles will radiate additional waves at frequencies different from the incoming ones (e.g., twice the incident frequency in the case of second harmonic generation). Many applications of NLO are based on this generation of an additional beam, as will be discussed further.

The realization of nonlinear optical interactions requires the use of intense optical fields because the nonlinear response of the medium is always low when the optical frequencies are far from the electronic resonant frequencies of the material. However, if the electric field is too intense an irreversible degradation of the material occurs.

NLO phenomena are most commonly observed with laser beams. As an example, the intensity emitted by pulsed lasers may easily reach 10^{10} W · cm^{-2}, with a corresponding electric field of 10^8 V · m^{-1}. It should be noted that this field remains a weak perturbation in comparison to the internal field binding the electrons, typically 3×10^{10} V · m^{-1}. Moreover, such high power levels are not a necessary condition for the observation of most of the NLO interactions. Under favorable conditions, discussed further, an intensity of 1 W · cm^{-2} of coherent light is sufficient to realize a second harmonic generation experiment.

If the intensity is lower than 10^{10} W · cm^{-2}, the induced polarization can be written as a Taylor series of the successive powers of the electric field.

The quadratic term of the induced polarization is responsible for 3-wave interactions of SFM and DFM. These effects are observed in media with a quadratic electric susceptibility, which means noncentrosymmetric materials. Actually, in a centrosymmetric medium, two opposite directions are equivalent, and so the polarization must change sign if the optical electric field is reversed. Then, there can be no even powers of the field in the expansion of the polarization in such media. In noncentrosymmetric materials, the associated response is strongly enhanced if the nonlinear polarization and the radiated electric field achieve a constructive interaction over all the dipoles. This condition requires the use of incident coherent optical fields; it is known in NLO as phase-matching, and it is only achievable in anisotropic crystals, as will be explained further. Nevertheless, quadratic nonlinear interactions may be realized in isotropic media, whether solid, liquid, or gas, as soon as they lack an inversion symmetry.

Another effect arising from the quadratic polarization is the linear electrooptic effect, also known as Pockels effect (1893). It is described as the interaction between two fields at optical frequency with one static or low frequency ($\leq 10^5$ Hz) electric field, which induces a modification of the refractive index. The Pockels cells, used for optical modulation, are based on an external applied low-frequency electric field.

On the other hand, an electric field can be photoinduced and involved in a linear electrooptic effect, which is called a photorefractive effect. It leads to self-focusing or defocusing of the beam in the material, which can be detrimental in regard to optical damages, or used for the propagation of optical spatial solitons.

The cubic term of the induced polarization is responsible for 4-wave interactions: frequency conversion with corresponding SFM and DFM, and the particular case of direct third harmonic generation, on the one hand, and phase conjugation which allows us to restore a distorted wavefront, on the other hand.

If the incident frequency is close to the electronic resonant frequencies of the medium, the nonlinear response is strongly enhanced. Resonant techniques such as multiphoton absorption and ionization or stimulated Raman scattering are used for spectroscopic applications. Because of maximal linear optical absorption at resonant frquencies, this is not an optimal situation for the generation of powerful beams. All the cubic and resonant NLO interactions are not within the scope of the present article, and details may be found in specialized books.

MAIN APPLICATIONS OF PARAMETRIC DEVICES

The function of optical parametric devices is to extend the wavelength range of lasers, which mainly emit discrete or limited-tuning-range wavelengths: optical parametric crystals are then associated with laser media in order to generate or amplify coherent light from 0.2 μm to 20 μm. Particularly interesting from the point of view of applications is the potential to realize all-solid-state tunable laser sources, with the association of nonlinear crystals with a solid-state laser pumped by a diode. As shown in Fig. 2, the nonlinear crystals can be placed outside or inside the laser cavity, and are called *extracavity* or *intracavity* devices, respectively; for extracavity devices, the parametric interaction can be resonant (by placing the nonlinear crystal in a resonant cavity) or nonresonant.

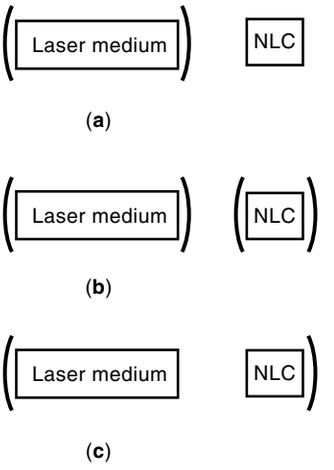

Figure 2. Configurations of association of a laser medium with an NLC: (a) extracavity nonresonant, (b) extracavity resonant, (c) intracavity.

A useable nonlinear crystal should present several other physical properties such as good transparency and low optical absorption at the concerned frequencies, high optical damage threshold, and mechanical and chemical stability.

Such systems have a high plug in efficiency. They offer a compact, reliable, powerful, and eventually portable alternative, whereas liquid and gas lasers are inconvenient. Moreover, integrated optoelectronic devices are now developed.

The field of application of parametric interactions is as wide as that of lasers themselves. Optical data storage, printing, eye-safe telemetry, machining, and medical laser systems are a few examples among those that clearly benefit from the wider wavelength range delivered by parametric devices. Tunable picosecond lasers also offer new capabilities in high repetition rate optical telecommunications through wavelength multiplexing and soliton propagation. Apart from these large-scale commercial applications, scientific applications are developed for parametric devices, especially in the field of spectroscopy: tunable femtosecond laser sources allow a variety of time-resolved studies.

The actual development of parametric devices allows us to fulfill all kinds of experimental requirements: apart from their wide wavelength range, they offer a variety of peak intensities, pulse widths (from the millisecond to the femtosecond ranges), and repetition rates.

INDUCED MACROSCOPIC POLARIZATION

We consider the most frequently encountered situation where the polarized units of the medium have negligible sizes compared with the optical wavelengths, the optical frequencies are far away from the resonance of the medium, and optical field intensities do not exceed a few gigawatts per square centimeter. We also suppose that the displacement of the optical fields lead to a corresponding time displacement of the induced polarizations, and the polarization effects are supposed to occur at the site of the polarizing field with no remote interactions.

Linear and Nonlinear Responses

In the framework of the approximations listed previously, the macroscopic electronic polarization of the unit volume of the

nonlinear medium, in the space and frequency domain ($\boldsymbol{r}$, ω), is usually expanded in a Taylor power series of the optical electric field according to (1):

$$\boldsymbol{P}(\boldsymbol{r},\omega)=\boldsymbol{P}_0(\boldsymbol{r})+\boldsymbol{P}^{(1)}(\boldsymbol{r},\omega)+\boldsymbol{P}^{(2)}(\boldsymbol{r},\omega)+\cdots+\boldsymbol{P}^{(n)}(\boldsymbol{r},\omega) \quad (1)$$

with

$$\boldsymbol{P}^{(n)}(\boldsymbol{r},\omega)=\epsilon_0\chi^{(n)}(\omega)\cdot\boldsymbol{E}(\boldsymbol{r},\omega_1)\otimes\boldsymbol{E}(\boldsymbol{r},\pm\omega_2)\otimes\cdots\otimes\boldsymbol{E}(\boldsymbol{r},\pm\omega_n) \quad (2)$$

- $\boldsymbol{P}_0(\boldsymbol{r})$ is the static polarization and $\boldsymbol{P}^{(n)}(\boldsymbol{r},\omega)$ stands for the nth-order polarization.
- $\omega=2\pi v=2\pi c/\lambda$ is the circular frequency associated with the frequency v and the wavelength λ.
- c is the light velocity in the vacuum.

The circular frequencies of the interacting waves verify the energy conservation:

$$\hbar\omega=\hbar\omega_1\pm\hbar\omega_2\pm\cdots\pm\hbar\omega_n \quad (3)$$

$\otimes$ stands for the tensorial product and $\cdot$ stands for the contraction between the nth-order susceptibility tensor $\chi^{(n)}(\omega)$ and the nth-order field tensorial product.

$\boldsymbol{P}^{(1)}(\boldsymbol{r},\omega)$ is the linear polarization and the $\boldsymbol{P}^{(n>1)}(\boldsymbol{r},\omega)$ are the nth orders of the nonlinear polarization. According to Eq. (2), the components of the first and second orders of the polarization vectors are expressed as

$$P_i^{(1)}(\boldsymbol{r},\omega)=\epsilon_0\sum_i\chi_{ij}^{(1)}(\omega)E_j(\boldsymbol{r},\omega) \quad (4)$$

$$P_i^{(2)}(\boldsymbol{r},\omega)=\epsilon_0\sum_{j,k}\chi_{ijk}^{(2)}(\omega)E_j(\boldsymbol{r},\omega_1)E_k(\boldsymbol{r},\pm\omega_2) \quad (5)$$

$\chi^{(2)}$ is expressed in meters per volt. The cartesian indices (i, j, k) refer to the optical frame (x, y, z), which is the orthonormal frame of the principal axes of the index ellipsoid and surface.

We consider plane waves, and we keep the complex form of the electric fields, which is given by

$$\boldsymbol{E}(\boldsymbol{r},\omega)=\boldsymbol{e}(\boldsymbol{k})E(\boldsymbol{r},\omega)\exp[j\boldsymbol{k}(\omega)\cdot\boldsymbol{r}] \quad (6)$$

- $E(\boldsymbol{r},\omega)=A(\boldsymbol{r},\omega)\exp[j\phi(\omega)]$ is the scalar complex amplitude where $\phi(\omega)$ is the initial phase.
- $E(\boldsymbol{r},-\omega)=E^*(\boldsymbol{r},\omega)$ because the fields are real.
- $\boldsymbol{e}$ and $\boldsymbol{k}$ are the unit electric field vector and the wave vector, respectively.

In an isotropic medium, the possible directions of $\boldsymbol{e}$ are all the directions in the plane normal to $\boldsymbol{k}$, and the modulus of $\boldsymbol{k}$ is the same in all directions. On the other hand, only two directions $\boldsymbol{e}^+$ and $\boldsymbol{e}^-$ are allowed in the plane normal to $\boldsymbol{k}$ with the corresponding moduli $|\boldsymbol{k}^+|$ and $|\boldsymbol{k}^-|$ in an anisotropic medium in the general case.

The two wave vectors $\boldsymbol{k}^+(\omega,\theta,\phi)$ and $\boldsymbol{k}^-(\omega,\theta,\phi)$ associated with a direction of propagation of unit vector $\boldsymbol{u}(\theta,\phi)$ are given by

$$\boldsymbol{k}^\pm(\omega,\theta,\phi)=\frac{\omega}{c}n^\pm(\omega,\theta,\phi)\boldsymbol{u}(\theta,\phi) \quad (7)$$

The spherical coordinates (θ, ϕ) of $\boldsymbol{u}$ in the optical frame (x, y, z) are related to the cartesian coordinates by

$$u_x=\sin\theta\cos\phi \qquad u_y=\sin\theta\sin\phi \qquad u_z=\cos\theta \quad (8)$$

We consider lossless media, thus, the refractive indices $n^\pm(\omega,\theta,\phi)=[\epsilon^\pm(\omega,\theta,\phi)]^{1/2}$, $n^+>n^-$, are real and correspond to the solutions of Fresnel (3):

$$\begin{aligned} n^\pm&=\left(\frac{2}{-B\pm(B^2-4C)^{1/2}}\right)^{1/2}\\ B&=-u_x^2(b+c)-u_y^2(a+c)-u_z^2(a+b)\\ C&=u_x^2bc+u_y^2ac+u_z^2ab\\ a&=n_x^{-2}(\omega),\qquad b=n_y^{-2}(\omega),\qquad c=n_z^{-2}(\omega)\end{aligned} \quad (9)$$

$n_x(\omega)$, $n_y(\omega)$, and $n_z(\omega)$ are the principal refractive indices of the index surface at the circular frequency ω. The existence of equalities between the principal refractive indices determines the three optical classes: isotropic ($n_x=n_y=n_z$) for the cubic system, uniaxial ($n_x=n_y=n_o\neq n_z=n_e$, o for ordinary and e for extraordinary) for the tetragonal, hexagonal and trigonal systems, and biaxial ($n_x\neq n_y\neq n_z$) for the orthorhombic, monoclinic, and triclinic systems. (n^+-n^-) is termed as birefringence.

The unit electric field vectors $\boldsymbol{e}^+$ and $\boldsymbol{e}^-$ are calculated from the propagation equation projected on the three axes of the optical frame. We obtain, for each wave, three equations that relate the three components (e_x, e_y, e_z) to the unit wave vector components (u_x, u_y, u_z):

$$(n^\pm)^2(e_p^\pm-u_p[u_xe_x^\pm+u_ye_y^\pm+u_ze_z^\pm])=(n_p)^2e_p^\pm \quad (10)$$

Here ($p=x$, y, and z) with $(e_x^\pm)^2+(e_y^\pm)^2+(e_z^\pm)^2=1$. Any parametric interaction occurs necessarily between the eigen modes $\boldsymbol{e}^+$ and $\boldsymbol{e}^-$ at the concerned frequencies.

Symmetry Properties of the Electric Susceptibility

In a lossless medium, any nth-order susceptibility tensor $\chi_{ij\ldots n}^{(n)}(\omega)$ is real [i.e., $\chi_{ij\ldots n}^{(n)}(\omega)=\chi_{ij\ldots n}^{(n)}{}^*(\omega)$], and it remains unchanged by concomitant permutations of the cartesian indices and the corresponding circular frequencies; that is to say, for $\chi^{(2)}$ (1),

$$\chi_{ijk}(\omega_3=\omega_1+\omega_2)=\chi_{jik}(\omega_1=\omega_3-\omega_2)=\chi_{kij}(\omega_2=\omega_3-\omega_1) \quad (11)$$

This property is called an *ABDP symmetry*. If the wavelength dispersion of the refractive indices of the nonlinear medium is small, $\chi^{(n)}$ is totally symmetric—the tensor is invariant with respect to any permutation of cartesian indices. This overall permutation symmetry is called *Kleinman symmetry,* which reduces the number of independent coefficients of the tensor from 27 to 10 for $\chi^{(2)}$. These properties are both intrinsic symmetry properties.

The symmetry of $\chi^{(n)}$ must correspond to that of the crystal in accordance with the Neumann principle (4). The application of this principle leads to a reduction of the number of independent coefficients and eventual connections between them. The form of $\chi^{(n)}$ is then specific of the crystal class (e.g., $\chi^{(2)}$ is nil for any centrosymmetric class).

ELECTROMAGNETIC ENERGY EXCHANGE

The time average work that is done by the electromagnetic waves in a nonlinear medium is one of the first ways to characterize the efficiency of a parametric interaction: the efficiency is maximum when the sign of the work remains positive over the distance of propagation. In that case, the nonlinear polarization $\boldsymbol{P}^{(n)}(\boldsymbol{r}, \omega)$ continuously transfers its energy to a wave $\boldsymbol{E}(\boldsymbol{r}, \omega)$ during a parametric interaction involving $(n + 1)$ waves. The work $W^{(n)}(\boldsymbol{r}, \omega)$ in a dielectric medium is given by (1):

$$W^{(n)}(\boldsymbol{r}, \omega) = 2\omega \,\mathrm{Im}[\boldsymbol{E}^*(\boldsymbol{r}, \omega) \cdot \boldsymbol{P}^{(n)}(\boldsymbol{r}, \omega)] \tag{12}$$

According to relations (5) and (6), the 3-wave work $W^{(2)}(\mathbf{r}, \omega_3 = \omega_1 + \omega_2)$ is equal to

$$W^{(2)}(\boldsymbol{r}, \omega_3) = 2\omega_3 \epsilon_0 \chi^{(2)}_{\mathrm{eff}}(\omega_3 = \omega_1 + \omega_2) \sin(\Delta\boldsymbol{k} \cdot \boldsymbol{r} + \Delta\phi) \tag{13}$$

The effective coefficient $\chi^{(2)}_{\mathrm{eff}}$ is given by

$$\chi^{(2)}_{\mathrm{eff}}(\omega_3 = \omega_1 + \omega_2) = \chi^{(2)}(\omega_3) \cdot \boldsymbol{F}^{(2)}(\omega_3 = \omega_1 + \omega_2) \tag{14}$$

with

$$\boldsymbol{F}^{(2)}(\omega_3 = \omega_1 + \omega_2) = \boldsymbol{e}^*(\omega_3) \otimes \boldsymbol{e}(\omega_1) \otimes \boldsymbol{e}(\omega_2) \tag{15}$$

$\boldsymbol{F}^{(2)}$ is the field tensor. Note that $\boldsymbol{e}^*(\omega_3) = \boldsymbol{e}(\omega_3)$ because the waves are linearly polarized. $\Delta\boldsymbol{k} \cdot \boldsymbol{r} + \Delta\phi$ is the phase parameter with

$$\begin{aligned} \Delta\boldsymbol{k} \cdot \boldsymbol{r} &= [\boldsymbol{k}(\omega_1) + \boldsymbol{k}(\omega_2) - \boldsymbol{k}(\omega_3)] \cdot \boldsymbol{r} \text{ and} \\ \Delta\phi &= \phi(\omega_1) + \phi(\omega_2) - \phi(\omega_3) \end{aligned} \tag{16}$$

Phase Relations

The sign of the work depends on the value of the phase parameter $\Delta\boldsymbol{k} \cdot \boldsymbol{r} + \Delta\phi$, which is the phase mismatch between the nonlinear polarization and the radiated wave.

- If $\Delta\boldsymbol{k} \cdot \boldsymbol{r} \neq 0$ and if there is no particular relation between $\Delta\boldsymbol{k}$ and $\Delta\phi$, then the work alternates in sign as a function of $\boldsymbol{r}$, which is a detrimental situation for the parametric interaction. The distance over which the work keeps the same sign is called the *coherence length* r_c. For the case where the three interacting waves have collinear wave vectors, we have $r_c = \pi/|\Delta\boldsymbol{k}|$, independently on $\Delta\phi$, according to Eq. (13). The coherence length depends only on the refractive indices. The typical values of r_c are very small, between 1 and 100 μm.
- Even if $\Delta\boldsymbol{k}$ and $\Delta\phi$ have values as in the previous case, it is possible to impose a constant sign for the work by applying a periodic phase correction equal to π after the waves have propagated over the coherence length. The periodic reset of π is classically achieved by changing the sign of the effective coefficient, which is called quasi-phase-matching (QPM): the nonlinear medium is then formed by a succession of thin crystal domains with a length equal to r_c (5).
- The best way to obtain a work with a sign constant over all the propagation distance is to have $\Delta\boldsymbol{k} \cdot \boldsymbol{r} = 0$. Furthermore, when at least one wave among the interacting waves is not incident in the nonlinear medium but is generated inside the nonlinear crystal, its initial phase is locked at the value that allows a maximum work, that is to say with $\Delta\phi = \pi/2$. Then in these conditions, the initial phases of a 3-wave parametric interaction verify $\phi(\omega_1) + \phi(\omega_2) = \phi(\omega_3) + \pi/2$. From the point of view of the quantum theory of light, the phase-matching of the waves corresponds to the total photon-momentum conservation; in other words,

$$\sum_{m=1}^{\gamma-1} \hbar\boldsymbol{k}(\omega_{\mathrm{m}}) = \hbar\boldsymbol{k}(\omega_\gamma) \tag{17}$$

with $\gamma = 3$ for a 3-wave interaction.

According to Eq. (7), the projection of the vectorial phase-matching relation (17) on the wave vector $\boldsymbol{k}(\omega_\gamma, \theta_\gamma, \phi_\gamma)$ at the highest circular frequency ω_γ is written:

$$\sum_{m=1}^{\gamma-1} \omega_m n(\omega_m, \theta_m, \phi_m) \cos\alpha_{m\gamma} = \omega_\gamma n(\omega_\gamma, \theta_\gamma, \phi_\gamma) \tag{18}$$

$\alpha_{m\gamma}$ is the angle between $\boldsymbol{k}(\omega_m, \theta_m, \phi_m)$ and $\boldsymbol{k}(\omega_\gamma, \theta_\gamma, \phi_\gamma)$. The circular frequencies verify the energy conservation: $\sum_{m=1}^{\gamma-1} \hbar\omega_m = \hbar\omega_\gamma$. The different $n(\omega, \theta, \phi)$ are the solutions n^+ and n^- given by Eq. (9). Collinear phase-matching corresponds to the case where all the interacting waves have collinear wave vectors (i.e., $\alpha_{m\gamma} = 0$ for each m wave).

Because any medium is dispersive [i.e., $\partial n(\omega)/\partial\omega \neq 0$], phase-matching can be achieved only in directions where the associated birefringence compensates the dispersion. In the case of normal dispersion [i.e., $n^{\pm}(\omega_i) < n^{\pm}(\omega_j)$ for $\omega_i < \omega_j$], only three types of combinations of the refractive indices verify equality (18) for a 3-wave parametric interaction. The three corresponding phase-matching relations in the collinear case are (6)

$$\omega_3 n^-(\omega_3, \theta, \phi) = \omega_1 n^+(\omega_1, \theta, \phi) + \omega_2 n^+(\omega_2, \theta, \phi) \tag{19}$$

$$\omega_3 n^-(\omega_3, \theta, \phi) = \omega_1 n^-(\omega_1, \theta, \phi) + \omega_2 n^+(\omega_2, \theta, \phi) \tag{20}$$

$$\omega_3 n^-(\omega_3, \theta, \phi) = \omega_1 n^+(\omega_1, \theta, \phi) + \omega_2 n^-(\omega_2, \theta, \phi) \tag{21}$$

Relations (19), (20), and (21) correspond, respectively, to types I, II, and III for the SFM ($\omega_3 = \omega_1 + \omega_2$), to types II, III and I for the DFM($\omega_1 = \omega_3 - \omega_2$) and to types III, I, and II for the DFM($\omega_2 = \omega_3 - \omega_1$). In a positive uniaxial crystal, the eigenmode n^+ corresponds to an extraordinary polarized wave and n^- to an ordinary one. These polarizations are reversed in a uniaxial crystal with a negative optical sign. The definition of extraordinary and ordinary waves is only valid in the principal planes of the index surface of biaxial crystals (3).

Symmetry Properties

According to relation (14), the effective coefficient not only is a function of the nonlinear optical properties $\chi^{(2)}$ but also depends on the linear optical properties via $\boldsymbol{F}^{(2)}$. Indeed, the unit electric fields are calculated from the refractive indices according to Eq. (10), and then the components of the field tensor are trigonometric functions of the direction of propagation. There exist particular relations between field tensor

components of SFM and DFM that are valid for any direction of propagation. Indeed the field tensor remains unchanged by concomitant permutation of the electric field vectors at the different frequencies and the corresponding cartesian indices, that is to say

$$\begin{aligned} F_{i\ j\ k}^{e_3 e_1 e_2}(\omega_3 = \omega_1 + \omega_2) &= F_{j\ i\ k}^{e_1 e_3 e_2}(\omega_1 = \omega_3 - \omega_2) \\ &= F_{k\ i\ j}^{e_2 e_3 e_1}(\omega_2 = \omega_3 - \omega_1) \end{aligned} \tag{22}$$

For a given interaction, the symmetry of the field tensor is governed by the vectorial properties of the unit electric field vectors, which is characteristic of both the optical class (isotropic, uniaxial, or biaxial) and the direction of propagation. These properties lead to a reduction of the number of independent components of the field tensor (3). Then the symmetries of the field tensor and of the electric susceptibility tensor are different, which can lead to a nil contraction between the two tensors, that is to say to a nil effective coefficient, even if the parametric interaction is phase-matched (i.e., $\Delta \boldsymbol{k} \cdot \boldsymbol{r} + \Delta\phi = 0$): the crystal classes D_4 (422) and D_6 (622) forbid the parametric interactions where two ordinary refractive indices and one extraordinary index are involved; it is also the case for two extraordinary and one ordinary refractive indices for the crystal classes C_{4v} (4 mm) and C_{6v} (6 mm).

Manley–Rowe Power Relations

The permutation symmetry relations in Eqs. (11) and (22) lead to relations between the effective coefficients of SFM and DFM. For a 3-wave process, we have

$$\chi_{\text{eff}}(\omega_3 = \omega_1 + \omega_2) = \chi_{\text{eff}}(\omega_1 = \omega_3 - \omega_2) = \chi_{\text{eff}}(\omega_2 = \omega_3 - \omega_1) \tag{23}$$

Equalities (23) allow us to establish relations between the corresponding works given by Eq. (12) in the case of a lossless medium. These relations are called Manley–Rowe power relations, which are written

$$\frac{W^{(2)}(\boldsymbol{r}, \omega_1)}{\omega_1} = \frac{W^{(2)}(\boldsymbol{r}, \omega_2)}{\omega_2} = -\frac{W^{(2)}(\boldsymbol{r}, \omega_3)}{\omega_3} \tag{24}$$

Because $\omega_3 = \omega_1 + \omega_2$, Eq. (24) leads to a work conservation condition, namely $W(\boldsymbol{r}, \omega_1) + W(\boldsymbol{r}, \omega_2) + W(\boldsymbol{r}, \omega_3) = 0$. Considering the example of SFM, this relation indicates that the total energy lost by the waves at ω_1 and ω_2 is transferred to the wave at ω_3.

NONLINEAR MATERIALS

The nonlinear medium for $\chi^{(2)}$ parametric interactions is a noncentrosymmetric crystal. No single nonlinear material is the best one for all applications, so the different crystals must be seen as complementary. Most parametric devices are based on inorganic crystals such as KH_2PO_4 (KDP), βBaB_2O_4 (BBO), LiB_3O_5 (LBO), $KNbO_3$, $LiIO_3$, $LiNbO_3$, $KTiOPO_4$ (KTP), $RbTiOAsO_4$ (RTA), $AgGaS_2$, $AgGaSe_2$, $ZnGeP_2$, and Tl_3AsSe_3 (7). The main organic crystals are Urea, 5-Nitrouracil (5-Nu), methyl-(2,4-dinitrophenyl)-aminopropanoate (MAP), 2-methyl-4-nitroaniline (MNA), 3-methyl-4-nitropyridine-*N*-oxyde (POM), *N*-(4-nitrophenyl)-L-propinol (NPP), and 2-amino-5-nitropyridine-dihydrogene phosphate (2A5NPDP) (8).

PROPAGATION OF THE WAVES IN THE NONLINEAR MEDIUM

The Maxwell equations describe the propagation of electromagnetic waves in a nonlinear medium. These waves are coupled through the nonlinear polarization, which we limit to the quadratic susceptibility term $\boldsymbol{P}^{(2)}(\boldsymbol{r}, \omega)$ in the present study. The material is supposed to be nonconducting, free of charges, nonmagnetic, and optically anisotropic, with low optical losses at the considered frequencies so that the $\chi^{(2)}$ tensor is real, as detailed previously.

General Propagation Equations for 3-Wave Mixing

We define an orthonormal frame (X, Y, Z) linked to the wave, with Z the direction of propagation of the waves, which are supposed to have collinear wave vectors in the following calculations. This frame must not be confused with the principal axes (x, y, z). To obtain the coupled differential equations that describe the 3-wave interaction, we generally neglect the backward propagating waves generated by the nonlinear polarization (9). This assumption, called the *slowly varying envelope approximation,* identically states that the field amplitudes have slow variations over one wavelength. This gives the following propagation equations (10):

$$\begin{aligned} \hat{M}_1 E_1 &= j\kappa_1 E_3 E_2^* \exp(j\,\Delta k \cdot Z) \\ \hat{M}_2 E_2 &= j\kappa_2 E_3 E_1^* \exp(j\,\Delta k \cdot Z) \\ \hat{M}_3 E_3 &= j\kappa_3 E_1 E_2 \exp(-j\,\Delta k \cdot Z) \end{aligned} \tag{25}$$

where the operator $\hat{\mathrm{M}}_i$ is given by

$$\begin{aligned} \hat{M}_i = \frac{\partial}{\partial Z} &+ \tan(\rho_{i_X})\frac{\partial}{\partial X} + \tan(\rho_{i_Y})\frac{\partial}{\partial Y} \\ &+ \frac{j}{2k_i}\left(\frac{\partial^2}{\partial X^2} + \frac{\partial^2}{\partial Y^2}\right) + \frac{1}{v_{g_i}}\frac{\partial}{\partial t} + \alpha_i \end{aligned} \tag{26}$$

where

- $E_i = E_i(X, Y, Z, t)$ is the Fourier component of the electric field at the circular frequency ω_i. We consider an interaction between linearly polarized waves, so that each field E_i corresponds to an eigen mode E^+ or E^- defined by relation (10).
- ρ_{i_X} and ρ_{i_Y} are the double refraction angles along the X and Y axes; because ρ_i varies with the frequency and the eigen mode, the three waves have different double refraction angles, and the beams do not overlap throughout all the crystal length. This phenomenon, called spatial *walk-off,* reduces the conversion efficiency of the interaction. It is important for small size beams. Actually, for parallel beams with a flat transverse profile and a beam radius w_0, the beams are completely separated after a distance $L_a = 2\,(w_o/\rho)$, with ρ in radians. In an uniaxial crystal, and in the principal planes of a biaxial crystal, three waves with collinear wave vectors have their Poynting vectors in the same plane [e.g., $(X–Z)$] so that the term $\tan(\rho_{i_Y})\,(\partial/\partial Y)$ is nil in operator $\hat{M}_i$. This is not the case out of the principal planes of a biaxial crystal.
- k_i is the wave vector modulus at ω_i. The second-order derivatives relative to the space coordinates is the diffrac-

tion term. It is important for beams with small transverse dimensions (typically if $w_0 \lesssim 50$ μm) and for real beams with nonuniform or distorted wavefronts.

- $v_{g_i} = (\partial\omega/\partial k)_{\omega=\omega_i}$ is the group velocity of the wave at ω_i. Because of the dispersion in wavelength of v_g, a temporal separation of the three waves occurs in the case of pulsed beams. The pulses at ω_i and ω_j are separated by a path equal to the initial pulse width after a distance $L_\tau = \tau/(v_{g_i}^{-1} - v_{g_j}^{-1})$, where τ is the pulse duration. The conversion efficiency saturates for longer crystal lengths. For the typical materials cited before, with a crystal length of 1 cm, this temporal walk-off becomes important for pulse durations shorter than 100 ps. For even shorter pulses, in the femtosecond range, we cannot consider constant group velocities in relation (26) for the interacting waves. The second term of the Taylor series $\epsilon(\omega)$ is added to the operator $\hat{M}_i$ to account for dispersion spreading. It is of the form $\frac{1}{2}(\partial^2 k/\partial\omega^2)_{\omega=\omega_i}$.
- α_i is the optical loss coefficient at the circular frequency ω_i. The linear absorption coefficient is given by $\alpha_i^L = \mathrm{Im}[\epsilon(\omega_i)] = \mathrm{Im}[\chi^{(1)}(\omega_i)]$. It must be low in order to achieve an efficient frequency conversion. The intrinsic part of α_i^L is low for wavelengths not too close to the edges of the transparency range of the nonlinear material. An extrinsic part of α_i^L is a result of the impurities and defaults induced by the synthesis of the material, which may also cause scattering losses. Both absorption and scattering are critical for high-power frequency converters. In the commonly used devices, α_i^L is less than $1\% \cdot \mathrm{cm}^{-1}$ at each wavelength. A nonlinear contribution α_i^{NL} is sometimes added to α_i. When the photon energy is greater than half of the band gap energy of the material, two-photon absorption occurs, and $\alpha_i^{NL} = \beta_i E_i^2$ in that case. α_i does not include the Fresnel reflection losses, which may reach 10% at each surface for each wave because Eqs. (25) deal with waves inside the nonlinear crystal. These losses must be considered in the final expressions of the optical powers outside the material. The crystal is then generally coated for maximum transmission at 1, 2, or 3 wavelengths in order to increase the conversion efficiency.
- $\kappa_i = \pi\chi_{\mathrm{eff}}/[n_i\lambda_i \cos^2(\rho_i)]$, where χ_{eff} (in meters per volt) is the effective coefficient defined in Eq. (14), n_i the refractive index corresponding to the considered eigenmode n^+ or n^- at the wavelength λ_i, and ρ_i the double refraction angle mentioned before.
- $\Delta k \cdot Z$ is the total phase-mismatch, expressed by relation (16), where the three wave vectors are collinear. For divergent beams, there exists a distribution of phase-mismatch resulting from noncollinear interactions between the angular components of the beams. In the most general case, Δk results from several contributions because many physical properties may affect the refractive indices of the material.

In the case of a nonnegligible optical absorption, the crystal is heated by the absorbed power, and the refractive indices vary because of the thermooptic effect, resulting in an additional phase-mismatch. One then must solve the heat conductivity equation simultaneously with the coupled differential equations (25). This has been extensively studied (11) but will not be considered hereafter.

The presence of optical rotation will also lead to a dephasing as a result of the dispersion in wavelength of the rotatory power. Nevertheless, for the most active crystals, this results in a slight and generally negligible shift of the phase-matching directions. The same kind of remarks hold for the photorefractive effect.

An external modification of the phase-mismatch is possible via the application of a static or low-frequency electric field (electrooptic effect) or heating or cooling of the crystal.

Finally, the chemical composition of the material also affects the phase-matching properties: the presence of chemical inhomogeneities, impurities, or defaults can lead to a variation of the refractive indices throughout the material. Depending on the considered material, the overall index homogeneity should reach $\pm 10^{-6}$/cm to achieve uniform phase-matching.

In the following discussions, we will neglect all the additional contributions to the phase-mismatch. For an interaction between three waves with collinear wave vectors, the different types are defined by relations (19)–(21). Note that the configurations of polarization that allow noncollinear phase-matching are the same as those for the collinear case but that the location of the corresponding phase-matching directions is different.

Resolution of the General Equations

The resolution of the coupled equations (25) begins by considering the relative importance of the relative terms in operator (26). It is easily done by evaluating the characteristic lengths L_τ and L_a detailed previously for the temporal and spatial walk-off, and $L_d = kw_0^2$ for diffraction. The effects whose characteristic length is long compared to the crystal length are not to be considered. Another simplification is possible in the case of small conversion efficiencies: the power of the incident beams remain constant, which is called *undepleted pump approximation*. Now there is only one differential equation left in system (25). The pump depletion may be evaluated by the characteristic length $L_{NL} = 1/[\kappa_3 \sqrt{E_1^2(0) + E_2^2(0) + E_3^2(0)}]$ where $E_i(0)$ is the incident electric field at ω_i (12).

In most cases, the integration of Eqs. (25) requires a numerical computation. Several studies have been made in particular situations: the most complete ones are pump depletion, diffraction, and spatial walk-off (13), as well as pump depletion and spatial and temporal walk-off (14). The models allow us to calculate the transverse beam profiles of the interacting waves and the conversion efficiencies in good agreement with corresponding experiments.

In order to make an analytical integration of Eqs. (25), we simplify the system by neglecting diffraction, spatial and temporal walk-off, and optical absorption. It is then written

$$\begin{aligned}
\frac{\partial E_1}{\partial Z} &= j\kappa_1 E_3 E_2^* \exp(j\,\Delta k \cdot Z) \\
\frac{\partial E_2}{\partial Z} &= j\kappa_2 E_3 E_1^* \exp(j\,\Delta k \cdot Z) \\
\frac{\partial E_3}{\partial Z} &= j\kappa_3 E_1 E_2 \exp(-j\,\Delta k \cdot Z)
\end{aligned} \tag{27}$$

with κ_i defined previously and $\rho_i = 0$ for the following.

This system allows us to study the principal effects (phase-matching and its related acceptance bandwidths, pump depletion) in the most commonly encountered situations. For the usual materials with a crystal length of 1 cm, this corresponds to a waist radius $w_0 \gtrsim 1$ mm and to a pulse duration $\tau \gtrsim 100$ ps. We mainly focus our attention on second harmonic generation (SHG) ($\omega + \omega = 2\omega$), which can be considered as the prototypical quadratic nonlinear interaction.

SECOND HARMONIC GENERATION

Integration of the Propagation Equations

The integration of the simplified system (27), according to the initial values of the different electric fields, allows us to calculate these fields at the exit surface of the nonlinear crystal, $E_i(X, Y, L)$, with L the crystal length. The power of each wave is obtained by integration of the intensity over the cross section of the beams. We will consider transverse TEM_{00} Gaussian profiles for the waves, expressed as

$$E_i(X,Y,Z) = E_{o_i}(Z)\exp\left(-\frac{X^2+Y^2}{w_i^2(Z)}\right) \tag{28}$$

where $w_i(Z)$ is the beam radius at $1/e$ of the electric field, which is identical to the radius at $1/e^2$ of the intensity. The minimum radius w_0, called the beam waist, is located at Z_0. $w(Z)$ is then given by

$$w^2(Z) = w_0^2\left(1+\frac{(Z-Z_o)^2}{Z_r^2}\right) \tag{29}$$

with $Z_r = \pi n w_0^2/\lambda$, the length over which the beam remains approximately collimated, called the *Rayleigh length*. If Z_r is much larger than the crystal length (i.e., $L/Z_r < 0.3$), we consider the beams to be parallel, with a constant radius w_0: this is the plane wave limit. For longer crystals, the beam radius cannot be regarded as constant, we have a longitudinal Gaussian profile. In the parallel beam limit, the integration over the transverse profile gives the following expression of the power at ω_i:

$$\begin{aligned} P_i(L) &= \frac{n_i}{2}\sqrt{\frac{\epsilon_0}{\mu_0}}\int\int |E_i(X,Y,L)|^2\,dX\,dY \\ &= n_i\sqrt{\frac{\epsilon_0}{\mu_0}}\frac{\pi}{4}\,w_0^2|E_{o_i}(L)|^2 \end{aligned} \tag{30}$$

The integration of the system (27) is independent of the time variations because we neglect the group velocity dispersion. Thus we calculate the instantaneous value of the electric fields. For continuous waves (c.w.), it is identical to the average power, but for pulsed beams, it is necessary to consider the pulse shape. A usual Gaussian dependence is described by

$$P_i(t) = P_{o_i}^c \exp\left(-2\frac{t^2}{\tau_i^2}\right) \tag{31}$$

and

$$\tilde{P}_i = \sqrt{\frac{\pi}{2}} f P_{o_i}^c \tau_i$$

where $P_{o_i}^c$ is the peak power at ω_i, τ_i is the half width at $1/e^2$, $\tilde{P}_i$ the average power, and f is the repetition rate.

Undepleted Pump Approximation in the Parallel Beam Limit

Equations (27) are integrated with the initial conditions: $\partial E_1^\omega/\partial Z = \partial E_2^\omega/\partial Z = 0$, and $E_3^{2\omega}(X, Y, 0) = 0$. The incident power at ω is distributed on the two eigenmodes $P_1^\omega(0)$ and $P_2^\omega(0)$. According to the relations in Eqs. (19)–(21), two configurations of polarization allow phase-matched SHG: type I where the two waves at ω are identically polarized, so $P_1^\omega(0) = P_2^\omega(0) = P_{tot}^\omega/2$, and type II, which is equivalent to type III, with two different polarizations at ω. In the crystal, at the entrance, these powers are $T_1^\omega P_1^\omega(0)$ and $T_2^\omega P_2^\omega(0)$, where $T_i = 4n_i/(1+n_i)^2$ is the Fresnel transmission coefficient. The initial electric fields $E_1^\omega(0)$ and $E_2^\omega(0)$ are deduced from these powers according to relation (30). We consider that the two fundamental beams have the same radius w_0^ω, which is not an approximation for type I SHG. The harmonic electric field is proportional to the product of the two fundamental fields, and then also has a Gaussain transverse profile, with the radius $w_0^{2\omega} = w_0^\omega/\sqrt{2}$. The harmonic power, obtained by Eqs. (27) and (30), is given in the SI system:

$$\begin{aligned} P^{2\omega}(L) &= BP_1^\omega(0)P_2^\omega(0)\frac{L^2}{w_0^2}\,\mathrm{sinc}^2\left(\frac{\Delta k\cdot L}{2}\right) \\ \text{with } B &= 9462\,\frac{2N-1}{N}\,\frac{\chi_{\text{eff}}^2 T_3^{2\omega}T_1^\omega T_2^\omega}{\lambda_\omega^2 n_3^{2\omega} n_1^\omega n_2^\omega} \end{aligned} \tag{32}$$

L is the crystal length in the direction of propagation.

N is the number of independently oscillating modes in the fundamental beam: every longitudinal mode at the harmonic pulsation can be generated by many combinations of two fundamental modes; the statistical calculation leads to the $(2N-1)/N$ factor (15).

λ_ω is the fundamental wavelength.

L, w_0, and λ are in meters; χ_{eff} is in meters per volt; B is in watt^{-1}. The refractive indices at the two wavelengths are $n_3^{2\omega} = n^-(2\omega)$; for type I SHG, $n_1^\omega = n_2^\omega = n^+(\omega)$, whereas for type II SHG $n_1^\omega = n^+(\omega) \neq n_2^\omega = n^-(\omega)$, according to relations (19)–(21). The SHG efficiency is defined as $\eta_{\text{SHG}} = P^{2\omega}(L)/[P_1^\omega(0) + P_2^\omega(0)]$. For c.w. beams, it is deduced from Eq. (32). For pulsed beams, this relation gives the peak power efficiency $\eta_{\text{SHG}}^{\text{pk}}$. One generally defines an additional average power conversion efficiency $\eta_{\text{SHG}}^{\text{av}} = \tilde{P}_{2\omega}(L)/\tilde{P}_\omega(0)$, which is equal to the ratio of the average pulse energies. For Gaussian temporal profiles, the harmonic pulse duration is shorter than the fundamental one, $\tau_{2\omega} = \tau_\omega/\sqrt{2}$, for the same reasons as the beam radii. The average power conversion efficiency is then smaller by a factor $\sqrt{2}$ than the peak power SHG efficiency.

Acceptance Bandwidths

According to Eq. (32), the generated harmonic power is maximum when the interference function $\mathrm{sinc}^2(\Delta k \cdot L/2)$ is equal to unity, which is possible only for $\Delta k = 0$. This phase-matching condition was previously established from energy exchange considerations.

At a given temperature T_{PM}, for a given fundamental wavelength λ_{PM} and configuration of polarization (type I or II), the relation $\Delta k = 0$ defines the phase-matching directions (θ_{PM},

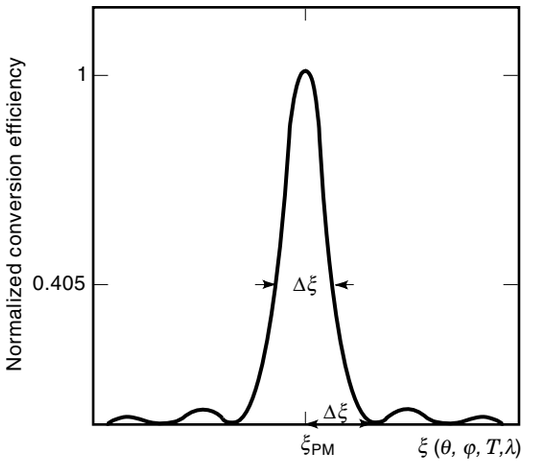

Figure 3. Conversion efficiency evolution as a function of ξ for a given crystal length. ξ denotes the angle θ or ϕ of the direction of propagation, the temperature T, or the wavelength λ. ξ_{PM} represents the considered parameter allowing phase-matching.

ϕ_{PM}), which lie on a cone, because of the symmetry of the index surface (6,16). In an uniaxial crystal, the refractive indices do not depend on ϕ, and so nor does θ_{PM}. The variation of θ_{PM} as a function of λ_{PM} is termed as the phase-matching tuning curve. Nevertheless, all the directions at constant θ_{PM} are not equivalent for SHG because the effective coefficient χ_{eff} depends on ϕ because of the variation of the field tensor $F^{(2)}$ elements, and so also the conversion efficiency. The situation is more complicated in the biaxial crystal, where θ_{PM} is not constant for different ϕ_{PM}. The fundamental wavelength ranges allowing phase-matching are different from one principal plane to the other, as are the associated SHG efficiencies.

For the study of real systems, it is important to know the effect of a deviation of Δk from 0 resulting from variations of the propagation angles ($\theta \pm \delta\theta$, $\phi \pm \delta\phi$), of the fundamental wavelength ($\lambda \pm \delta\lambda$) and of the temperature ($T \pm \delta T$) on the conversion efficiency. These evolutions are usually characterized by the associated acceptance bandwidths $\Delta\xi(\xi = \theta, \phi, \lambda, T)$. According to the variation of the conversion efficiency with ξ, plotted on Fig. 3, the acceptance bandwidth $\Delta\xi$ is defined as the full width at 0.405 of the maximum of $P^{2\omega}(\xi)$. $\Delta\xi$ is then the deviation from the phase-matching value ξ_{PM} leading to a phase-mismatch variation Δk from 0 to $2\pi/L$.

A larger value of $L\Delta\xi$ corresponds to a smaller decrease in the conversion efficiency for the same heating of the crystal (due to absorption or external heating) or for the same angular or wavelength shift resulting from the divergence and spectral linewidth of the fundamental laser beam, respectively.

$L\Delta\xi$ is a characteristic of the phase-matching direction. It is linked to the thermal, spectral, and angular dispersion of the refractive indices. The derivation of $L\Delta\xi$ is made by expanding Δk in a Taylor series about ξ_{PM}:

$$\frac{2\pi}{L} = \Delta k = \sum_{\xi=\theta,\phi,\lambda,T} \left\{ \left.\frac{\partial(\Delta k)}{\partial\xi}\right|_{\xi_{PM}} \Delta\xi + \frac{1}{2}\left.\frac{\partial^2(\Delta k)}{\partial\xi^2}\right|_{\xi_{PM}} (\Delta\xi)^2 + \cdots \right\} \tag{33}$$

When the second- and higher-order derivatives in Eq. (33) are negligible, the phase-matching is called critical (CPM) because $L\Delta\xi \approx |2\pi/[\partial(\Delta k)/\partial\xi|_{\xi_{PM}}]|$ is small. For the particular cases where $\partial(\Delta k)/\partial\xi|_{\xi_{PM}} = 0$, $L\Delta\xi = \sqrt{|4\pi L/[\partial^2(\Delta k)/\partial\xi^2|_{\xi_{PM}}]|}$ is larger than CPM acceptance, and the phase-matching is called noncritical (NCPM) for the considered parameter ξ.

We consider each parameter independently, holding the other constant and equal to the phase-matching value.

The angular acceptances are calculated from the relation in Eq. (33), with the refractive indices given by Eq. (9), according to the phase-matching relations in Eqs. (19)–(21). At a given temperature T_{PM} and wavelength λ_{PM}, θ_{PM} does not depend on ϕ in a uniaxial crystal, so the associated angular acceptance $L\Delta\phi$ is infinite, but $L\Delta\theta$ is finite. The angular noncritical phase-matching corresponds to a SHG in the principal plane, at $\theta = \pi/2$. For biaxial crystals, $L\Delta\phi$ is not infinite, but the anisotropy of the angular acceptances remains. The phase-matching is angular noncritical along the three principal axes (x, y, z) of the index surface, which is easily established by considering the symmetry of this surface (16).

The anisotropy of the angular acceptances leads to an intensity anisotropy of the harmonic beam. A fundamental beam with a circular cross section generates a beam at 2ω with an elliptic cross section. The small and large axes are respectively contained in the planes of critical and noncritical angular acceptances. This anisotropy of the harmonic beam is then strongly reduced for angular noncritically phase-matched SHG.

Critical acceptances are small, about 1 mrad · cm. For example, in the uniaxial crystal KDP, type I SHG is phase-matched at $\theta_{PM} = 41.2°$ for $\lambda_{PM} = 1.064$ μm, and the associated critical angular acceptance is $L\Delta\theta = 2.0$ mrad · cm. For a fundamental wavelength $\lambda_{PM} = 0.5175$ μm, type I SHG is noncritical (i.e., $\theta_{PM} = 90°$), and the NCPM angular acceptance is $L\Delta\theta = 41$ mrad · cm. Furthermore, the second benefit of this NCPM is that the associated walk-off angle is nil. Consequently, no attenuation of the conversion efficiency occurs.

The thermal acceptance bandwidth is calculated according to the relation in Eq. (33) for fixed propagation angles (θ_{PM}, ϕ_{PM}) and fundamental wavelength (λ_{PM}). Small thermooptic coefficients $\partial n_i/\partial T$ lead to a large thermal acceptance. For SHG at $\lambda_{PM} = 1.064$ μm, $L\Delta T$ varies from 0.3 K · cm for $KNbO_3$ to 51 K · cm for βBaB_2O_4. Nonlinear crystals with a small thermal acceptance need to be thermalized to avoid important fluctuations of the generated harmonic power, especially when the optical absorption at the concerned frequencies is not negligible.

The spectral acceptance is an important issue for fundamental lasers emitting with a large bandwidth. For the usual nonlinear materials, $L\Delta\lambda$ is about 1 nm · cm, which is larger than the linewidth of many laser lines, except for subpicosecond lasers.

When $\partial(\Delta k)/\partial\lambda|_{\lambda_{PM}} = 0$, the phase-matching is noncritical with respect to the wavelength and is termed as λ-noncritical. In that case, the group velocities are matched along the direction of propagation, and temporal walk-off is avoided.

The angular and spectral NCPM are linked by the phase-matching tuning curve $\lambda_{PM} = f(\theta_{PM})$. The angular NCPM corresponds to a nil derivative $\partial\lambda_{PM}/\partial\theta_{PM} = 0$, as shown on Fig. 4(a) at the point (λ^0_{PM}, θ^0_{PM}). Actually, a deviation of θ^0_{PM} at constant λ_{PM} leads to a minimum departure from the phase-matching curve. At this point, $\partial\theta_{PM}/\partial\lambda_{PM}$ is infinite, and the phase-

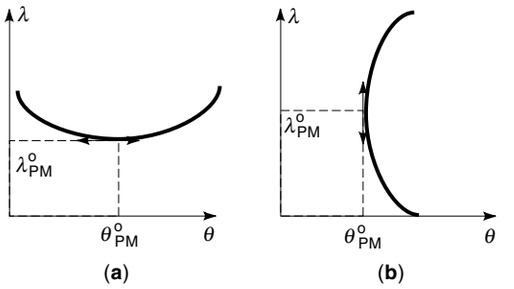

Figure 4. Schematic phase-matching tuning curve $\lambda_{PM} = f(\theta_{PM})$. The point $(\lambda^{\circ}_{PM}, \theta^{\circ}_{PM})$ corresponds to (a) angular noncritical phase-matching or (b) λ-noncritical phase-matching.

matching is a spectral critical one. Figure 4(b) shows the reciprocal case: at $(\lambda^{\circ}_{PM}, \theta^{\circ}_{PM})$ the phase-matching is λ-noncritical and thus angular critical (8).

Spectral NCPM is important for subpicosecond lasers, which have large linewidths and suffer from group velocities dispersion. Angular NCPM is suitable for strongly focused beams. Particular noncollinear configurations may then be used to enhance the acceptance bandwidths when collinear phase-matching is critical. One-beam noncritical noncollinear phase-matching is noncritical with respect to the angle of one of the input beams (17). Vectorial group noncollinear phase-matching is noncritical with respect to the wavelength of one of the beams (18).

SHG with Spatial Walk-off

The double refraction angles of the three interacting waves are generally not equal, so that the spatial overlap of the beams is reduced and the SHG conversion efficiency is attenuated. Types I and II SHG are not equivalent with respect to this effect. For type I, the two fundamental waves have identical polarization and thus their double refraction angles are equal and different from the harmonic one. For type II SHG, the two fundamental double refraction angles are different and the beams are totally separated beyond a propagation distance L_a. This is illustrated on Fig. 5. Apart from the attenuation of the conversion efficiency, spatial walk-off is responsible for a distorted transverse profile of the generated wave: the harmonic beam is larger than the fundamental one for type I, in contrast to type II.

We assume that the three double refraction angles ρ_i are coplanar, which is not an approximation in the uniaxial crystal and in the principal planes of the biaxial crystal. The 3-wave interaction is then described by the system in Eq. (27), with one more term $\tan(\rho_{i_x})\ \partial/\partial X$. The walk-off angle is defined as the maximum difference between these double refraction angles, $\rho = \mathrm{Max}(|\rho_i - \rho_j|)$ with $i \neq j = 1$, 2, or 3. For the common nonlinear materials, the maximum walk-off angles are less than 4°. The integration of the propagation equation in the undepleted pump approximation gives the harmonic power:

$$P^{2\omega}(L) = BP^{\omega}_1(0)P^{\omega}_2(0)\frac{L^2}{w_0^2}\frac{G(L, w_o, \rho, \Delta k)}{\cos^2 \rho_{2\omega}} \qquad (34)$$

- In the parallel beam limit (i.e., $L/Z_r < 0.3$), we have $G(L, w_0, \rho, \Delta k) = g(\sigma)\ \mathrm{sinc}^2(\Delta k \cdot L/2)$ with $\sigma = \rho L/w_0$. The conversion efficiency is then maximum for perfect phase-matching (i.e., $\Delta k = 0$). However, for type II SHG, the separation of the fundamental beams reduces the effective interaction length and leads to a saturation of the associated acceptance bandwidths, which is not the case for type I.

Analytical expressions of g are obtained only in the asymptotic cases (19,20). For perfect phase-matching, we have

if $\sigma \ll 1$, corresponding to low walk-off or low focusing, $g \approx 1$ for both types I and II; thus $P^{2\omega}_{I,II}(L) \propto L^2$,

if $\sigma \gg 1$, for type I $g_I \propto 1/\sigma$ and $P^{2\omega}_I(L) \propto L/\rho$; for type II $g_{II} \propto 1/\sigma^2$. Thus $P^{2\omega}_{II}(L)$ reaches a saturation value $P^{2\omega}_{II_{sat}}(L) = (1.351/\rho^2)\ BP^{\omega}_1(0)P^{\omega}_2(0)$ because of the complete separation of the fundamental beams.

Type I SHG is then more suitable than type II for strong focusing applications in the parallel beam limit.

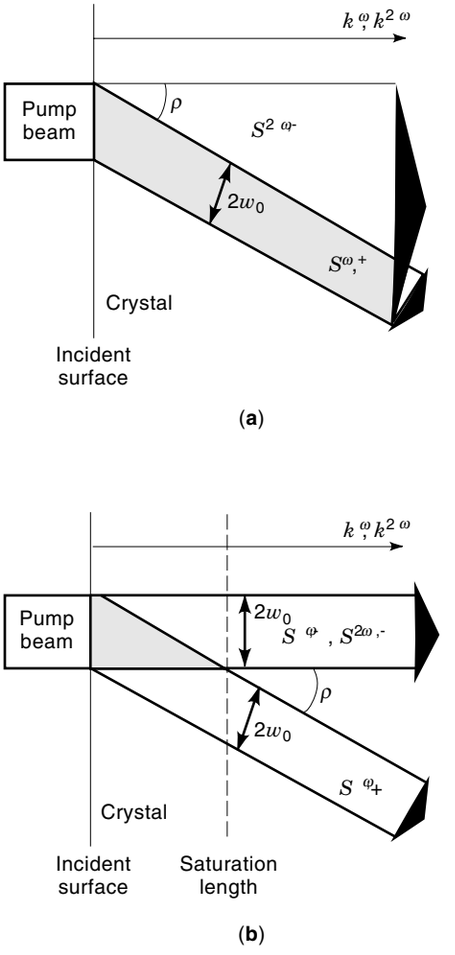

Figure 5. Schematic beam separation in the parallel beam limit for (a) type I SHG and (b) type II SHG. $\boldsymbol{S}$ are the Poynting vectors, and $\boldsymbol{k}$ are the associated wave vectors collinear to the CPM direction. + and − refer to the eigenmodes n^+ and n^-. The shaded area denotes the volume of interaction, whereas the black arrows refer to the interacting beams.

Such a difference between the two types of SHG also exists in the case of temporal walk-off for short pulses: type II leads to a saturation of the conversion efficiency, in contrast to type I.

- For longitudinal Gaussian beams, the attenuation factor is $G(L, w_0, \rho, \Delta k, f)$, where f gives the position of the beam waist inside the crystal: $f = 0$ at the entrance and $f = 1$ at the exit surface. A numerical computation is required for the calculation of G (21).

The maximum value of $P^{2\omega}$ is found for nonzero phase-mismatch $\Delta k_{opt} \neq 0$ as a result of noncollinear interactions imposed by the pump divergence. The optimum location of the beam waist is always at the center of the crystal $f_{opt} = 0.5$ for type I, whereas for type II it comes nearer to the entrance surface as the focusing is increased ($f_{opt} \to 0$ if $L/Z_r \uparrow$).

We plot on Fig. 6 the calculated SHG efficiency corresponding to the optimum phase-mismatch and waist location, Δk_{opt} and f_{opt}. This gives a clear illustration of the walk-off effect in usual harmonic generators with nonnegligible focusing.

For a zero walk-off angle, the evolution is similar for both types of SHG. An optimum focusing is found at $L/Z_r = 5.68$, which defines the optimum waist radius for given crystal length, or the optimum length for fixed waist radius. The definition of the optimum focusing conditions must take into account the damage threshold of the material, which gives the lower limit of the beam waist radius. The decreasing efficiency for stronger focusing is a result of the variation of the associated "average beam radius" inside the crystal, which increases for $L/Z_r > 5.68$.

In the case of nonzero walk-off angles, type I and type II exhibit different behaviors. The calculation of the conversion efficiency as a function of the crystal length, for a fixed beam radius, shows a saturation for type II, in contrast to type I. In the case of a fixed crystal length, the optimum focusing for type I corresponds to smaller values of $(L/Z_r)_{opt}$ if the walk-off angle increases, and the associated maximum efficiency becomes smaller. For type II, an optimum focusing becomes less and less apparent while $(L/Z_r)_{opt}$ shifts to much smaller values than for type I for the same variation of ρ; the decreasing of the maximum amplitude is stronger in the case of type II.

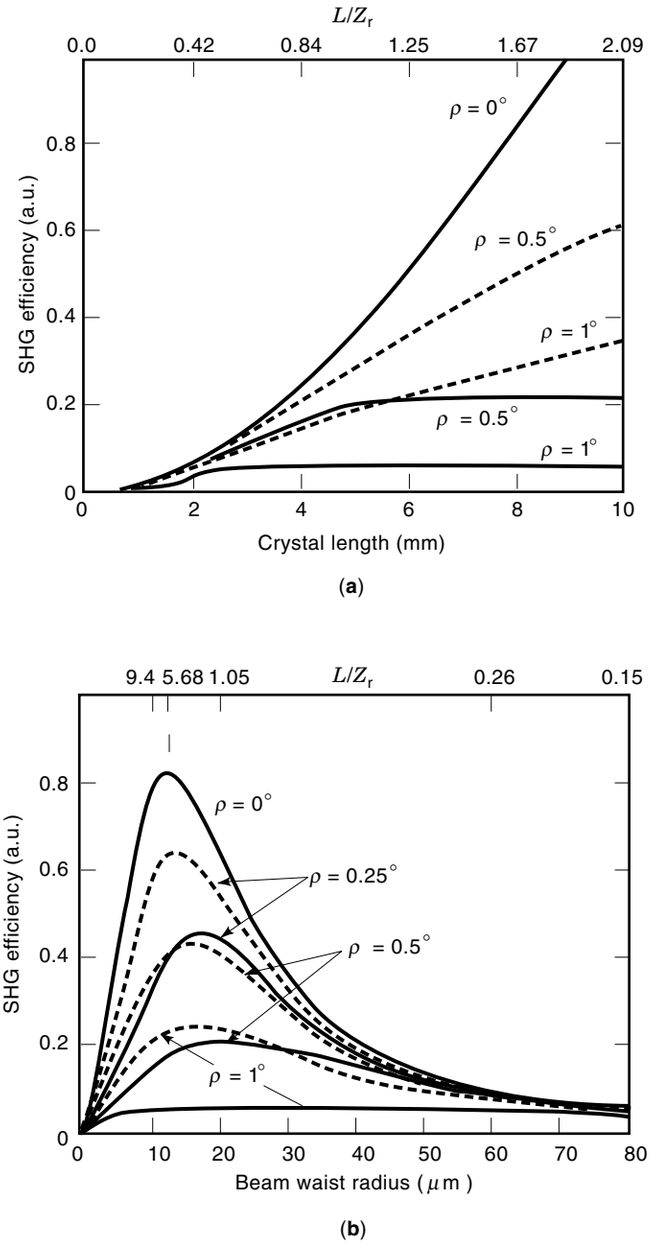

Figure 6. Type I (dashed curves) and type II (solid lines) SHG conversion efficiencies calculated as a function of L/Z_r for different typical walk-off angles ρ: (a) corresponds to a fixed focusing condition ($w_o = 30$ μm) and (b) is plotted for a constant crystal length ($L = 5$ mm). All the calculations are performed with the same effective coefficient, refractive indices, and fundamental power.

For type II SHG devices with strong focusing conditions, walk-off compensation is needed. It is achievable by two possible ways:

- Noncollinear phase-matching is used such as the angle between the two fundamental wave vectors inside the nonlinear crystal is equal to the walk-off angle ρ. The associated Poynting vectors are then parallel, and the harmonic beam is at an angle about $\rho/2$. This interaction is angular noncritical with respect to one fundamental beam, and type II is turned into a pseudotype I SHG because the saturation of the efficiency is avoided (22).
- Two crystals with the same length and cut in the same CPM direction are associated. The second crystal is rotated 180° with respect to the first one around the direction of propagation or around the direction orthogonal to the direction of propagation and contained in the walk-off plane. The beams are separated into the first crystal and then converge into the second one. In fact, n groups of two such crystals, of individual length L, can be assembled and optically contacted in order to avoid Fresnel reflection losses. The associated effective walk-off angle is much lower than that of a single crystal of length $2nL$; this allows an enhancement of the SHG efficiency

by one or two orders of magnitude with n ranging between 1 and 6 (23). Unfortunately, the realization of good-quality optical contacts is difficult.

SHG with Pump Depletion

For pulsed beams with high peak intensities or tight focusing SHG devices, important values of the conversion efficiency are reached. For example, a 7 mm long KTP crystal produces 80% energy conversion efficiency for the SHG of an injection-seeded, single longitudinal mode Nd : YAG laser emitting 900 mJ pulses at 1.064 μm with a 8 ns duration (full width at half maximum) and to 10 Hz repetition rate (24). With the same material, it is possible to generate very high average powers: up to 100 W of 0.532 μm radiation is obtained from 200 W of fundamental power, with 2.5 kHz repetition rate and 25 ns pulsewidth (25).

As soon as $\eta_{\mathrm{SHG}}^{\mathrm{pk}}$ is greater than 10%, the pump beam cannot be regarded as undepleted, and the formula in Eq. (32) is no more valid. We must then integrate the complete system in Eq. (27); we consider the case of negligible walk-off attenuation, which in fact is the suitable case to achieve high conversion efficiency. The electric fields at the exit surface of the crystal are expressed in terms of Jacobian elliptic functions $\mathrm{sn}(u, m)$, where the parameter m must not be confused with the modulus, $k = \sqrt{m}$, of the function (1,11,26). In the case of type I SHG, the generated harmonic intensity is expressed as

$$I^{2\omega}(X,Y,L) = I^{\omega}_{\mathrm{tot}}(X,Y,0)T^{2\omega}T^{\omega}v_{\mathrm{b}}^2\mathrm{sn}^2\left(\frac{\Gamma(X,Y)L}{v_{\mathrm{b}}}, v_{\mathrm{b}}^4\right) \quad (35)$$

with $I^{\omega}_{\mathrm{tot}}(X, Y, 0)$ the total incident fundamental power, and

$$\frac{1}{v_{\mathrm{b}}} = \frac{\Delta s}{4} + \sqrt{1+\left(\frac{\Delta s}{4}\right)^2}$$

$$\text{with } \Delta s = \frac{k^{2\omega}-k^{\omega}}{\Gamma} \text{ and } \Gamma(X,Y) = \kappa_3\sqrt{\frac{I^{\omega}_{\mathrm{tot}}(X,Y,0)T^{\omega}}{2n}}\sqrt{\frac{\mu_0}{\epsilon_0}}$$

$n = n^{\omega} = n^{2\omega}$ for type I SHG, and the other parameters defined previously. The intensity of the fundamental beam at the exit of the crystal is easily established from the Manley–Rowe relations in Eq. (24).

The effect of a nonzero phase-mismatch is much more complicated in the case of pump depletion. The associated acceptance bandwidths, calculated from the relation in Eq. (35), decreases with increasing ΓL (26). This is of particular importance for high-power devices: the residual absorption leads to a heating of the crystal. Together with the beam divergence, they can create an important dephasing.

Because of the periodic nature of the Jacobian elliptic functions, there exists an optimum value of $(\Gamma L)_{\mathrm{opt}}$ beyond which the harmonic intensity decreases. The computation of $(\Gamma L)_{\mathrm{opt}}$ for the considered phase-matching direction allows us to determine the optimum incident intensity $I^{\omega}_{\mathrm{opt}}$ for a given crystal length or the optimal length L_{opt} for a given fundamental beam. This must take into account the damage threshold of the nonlinear material I_{dam}, which imposes an upper limit to the incident intensity.

For perfect phase-matching, $\Delta k = 0$, we have $\Delta s = 0$ and $v_{\mathrm{b}} = 1$, and the Jacobian elliptic function $\mathrm{sn}(u, 1)$ is equal to $\tanh(u)$: the conversion efficiency asymptotically approaches 100% with the complete depletion of the pump. It is not achievable in real cases because there always exist a residual dephasing, which is a result of the divergence of the beam for example. For small ΓL, the functions $\tanh^2(\Gamma L) \approx \Gamma^2 L^2$ and $\mathrm{sn}^2(\Gamma L/v_{\mathrm{b}}, v_{\mathrm{b}}^4) \approx \sin^2(\Gamma L/v_{\mathrm{b}})$ with $v_{\mathrm{b}} \approx 2/\Delta s$. So, in that case, the integration of the intensity over the cross section of the beam exactly leads to the formula in Eq. (32), which is established in the undepleted pump approximation.

For type II SHG, the expression of $I^{2\omega}(L)$ is more complicated and is only given for perfect phase-matching here:

$$I^{2\omega}(L) = 2I^{\omega}_1(0)T^{2\omega}_3T^{\omega}_1\mathrm{sn}^2\left(\Gamma_{\mathrm{II}}L, \frac{I^{\omega}_1(0)}{I^{\omega}_2(0)}\right) \quad (36)$$

$$\text{with } \Gamma_{\mathrm{II}} = \kappa_3\sqrt{\frac{n^{2\omega}_3T^{\omega}_2I^{\omega}_2(0)}{n^{\omega}_1n^{\omega}_2}}\sqrt{\frac{\mu_0}{\epsilon_0}}$$

with $I^{\omega}_1(0) \le I^{\omega}_2(0)$. The parameter $I^{\omega}_1(0)/I^{\omega}_2(0)$ is termed as photon imbalance.

Thus, even for perfect phase-matching, the efficiency will not reach 100% if the two incident intensities are not strictly equal. Note that a circularly polarized fundamental wave will allow an easier realization of a unit photon imbalance than a linearly polarized one. On the other hand, for crystals with anisotropic losses or with an important birefringence, the optimum input polarization does not lie exactly at $\pi/4$ of the principal axes but rather slightly shifted.

All the previous intensities are peak intensities in the case of pulsed beams, which are generally used for high conversion efficiency SHG. For a fundamental beam with a flat transverse profile, the integration of the previous intensities over the cross section is obvious, and the harmonic exhibits the same profile and radius as the incident beam. The SHG conversion efficiency is then directly derived from the relations in Eq. (35) and (36). The possible variations as a function of ΓL are plotted on Fig. 7.

For a fundamental beam with a transverse Gaussian profile, the depletion induces an important variation of the beam profiles along the interaction length (12). Actually, the depletion is more important in the center of the beam, where the fundamental intensity is maximum, than on the edges, corresponding to low intensity.

For type I SHG without dephasing, and for type II SHG with equal intensities for the two eigenmodes, the harmonic beam keeps a Gaussian transverse profile, but the associated radius changes over the propagation: from $w^{\omega}_0/\sqrt{2}$ at the entrance of the crystal where pump depletion as not already occurred to w^{ω}_0 at the length where the pump is completely depleted. In other cases, where the parameter in the Jacobian elliptic function is not equal to unity, the harmonic beam rapidly deviates from a transverse Gaussian profile. In all cases, the harmonic power deduced by the integration of relations (35) and (36) over the cross section of the beam has a different variation than with flat profiles. $P^{2\omega}(L)$ is still a periodic function with respect to L, but it never turns back to zero when L increases. A typical evolution of the transverse profiles and conversion efficiency is shown in Fig. 8.

Once again these considerations concern the peak intensities and powers. The integration of the previous results over the temporal profiles will give the pulse energies. The evolution of the temporal profiles for flat transverse beams is identical to that of the transverse peak profiles. In all cases, the

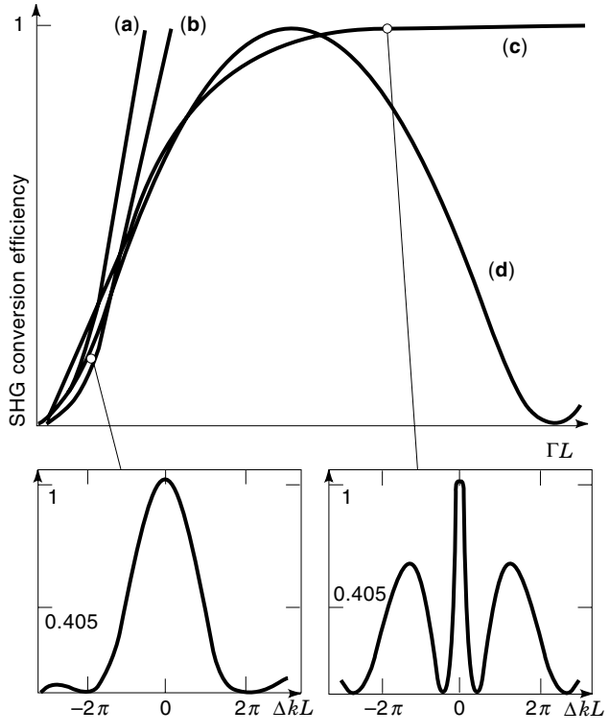

Figure 7. Schematic peak conversion efficiencies for flat transverse profiles, corresponding to (a) no depletion, no dephasing $\eta_{SHG} = \Gamma^2 L^2$; (b) no depletion, dephasing $\eta_{SHG} = \Gamma^2 L^2 \mathrm{sinc}^2\delta$; (c) depletion, without dephasing $\eta_{SHG} = \tanh^2 \Gamma L$; (d) depletion and dephasing (type I SHG) or depletion and nonunity photon imbalance (type II SHG) $\eta_{SHG} = \eta_m \mathrm{sn}^2(\Gamma L/v_b, m)$. For a fixed crystal length, ΓL is proportional to the fundamental intensity, and for constant $I^{\omega}(0)$, ΓL is proportional to the length L.

relation between the energy and peak conversion efficiencies is not given by the simple ratio $\eta^{av}_{SHG} = (\tau^{2\omega}/\tau^{\omega})\ \eta^{pk}_{SHG}$ in contrast to undepleted SHG.

Quasi-Phasematching

According to Eq. (32) the generated harmonic power has a quadratic dependency to the crystal length ($P^{2\omega} \propto L^2$) for a phase-matched interaction. When the dispersion in wavelength of the refractive indices does not allow birefringence phase-matching, the harmonic power oscillates with the periodicity $2r_c$, where r_c the coherence length previously mentioned. In that case, quasi-phase-matching is used to increase continuously the harmonic power inside the nonlinear material, owing to a reverse of the nonlinear polarization every r_c. In the most general case, the switch of the nonlinear polarization can be done after an odd number of r_c. For such mth-order QPM, the periodicity of the structure is $2mr_c$. The equivalent nonlinear coefficient is $\chi_{QPM} = 2\chi_{eff}/(m\pi)$, where χ_{eff} is the effective coefficient, defined by relation (14), associated to the considered configuration of polarization and direction of propagation. The SHG efficiency is then reduced by a factor of $[2/(m\pi)]^2$ relative to birefringence phase-matching (5). When it is possible, first-order QPM is preferred to higher orders in the most general cases. Corresponding variations of the harmonic power with respect to the crystal length are shown in Fig. 9.

QPM offers specific advantages when compared to birefringence phase-matching. It may be used for any configuration of polarization; in particular, frequency conversion involving three parallel polarized waves are allowed, which is impossible by classical index matching. It is then possible to solicit the diagonal elements of the $\chi^{(2)}$ tensors, which often are their greatest elements. For example, in $LiNbO_3$, χ_{zzz} (-54 pm/V at $\lambda = 0.532\ \mu$m) is six times greater than the elements involved in type I or type II phase-matching (7).

Another advantage of QPM is that the direction of propagation may be controlled. In uniaxial materials, the QPM structure is realized for propagation in the principal plane, whereas in biaxial crystals the principal axes are used so that the associated walk-off angles are nil.

Finally, QPM allows frequency conversion at any wavelength in the transparency range of the nonlinear material and thus allows us to extend the tuning ranges of the existing materials. This is of particular interest for short wavelengths SHG for which phase-matching is not always possible. For

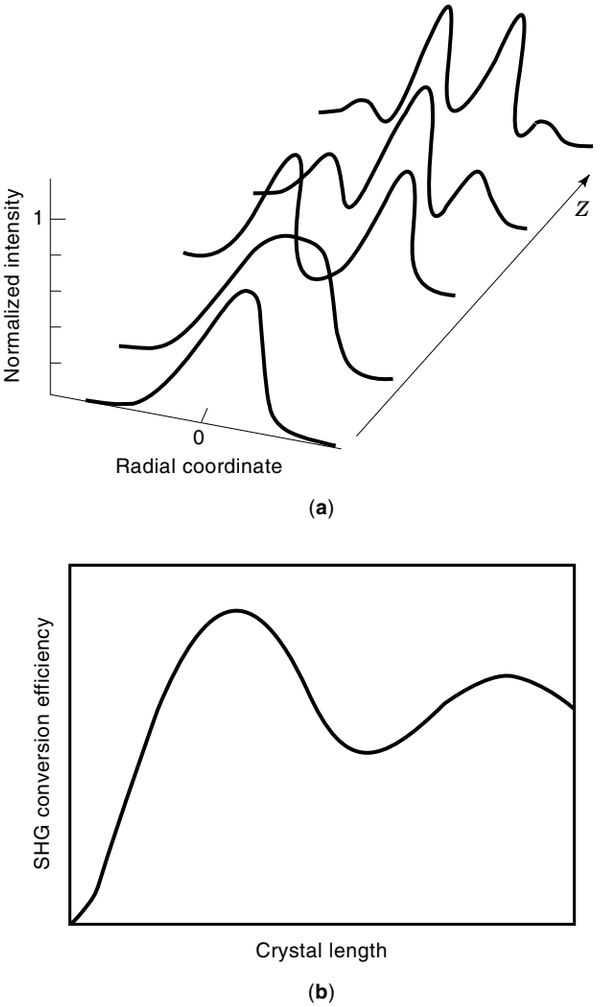

Figure 8. Schematic normalized transverse profile of the fundamental or harmonic beam over the interaction length: (a) peak intensities for the typical case of type II SHG with nonunity photon imbalance and (b) corresponding peak conversion efficiency as a function of the crystal length.

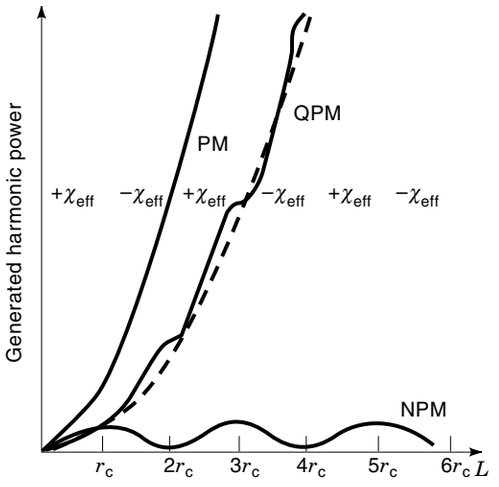

Figure 9. Spatial growth evolution of second harmonic conversion efficiency for non-phase-matching (NPM), $\Delta k \neq 0$, and phase-matching (PM), $\Delta k = 0$, in a "continuous" crystal, and for first-order quasi-phase-matching (QPM) in a periodic structure. The dashed line curve corresponds to $(4/\pi^2)\eta_{PM}(Z)$ where η_{PM} is the conversion efficiency of the phase-matched SHG deduced from Eq. (32). $r_c = \pi/\Delta k$ is the coherence length.

example, a $LiTaO_3$ structure with a domain period of 1.31 μm generates harmonic power down to $\lambda = 0.325$ μm (27).

Different techniques are employed for the practical realization of the QPM structures:

- For infrared conversion processes, the associated coherence lengths are large, on the order of 100 μm. It is then possible to bind thin plates of the nonlinear material, each rotated 180° with respect to the previous plates. For example, such GaAs structures are used for the SHG of a fundamental CO_2 laser emitting near $\lambda = 10$ μm.
- For ferroelectric materials (i.e., materials with a nonzero static polarization), periodic poling is an attractive way to realize QPM because the reverse of the ferroelectric domain is associated with a sign change of the nonlinear polarization. This periodic domain structure is generally obtained by applying an electric field to the sample through a periodic electrode.
- For waveguide applications, a ferroelectric domain structure can also be induced by proton- or ion-exchange or by electron beam scanning. Such devices are used to enhance the single-pass conversion efficiency of low-power lasers, especially c.w. lasers. Actually, because of the modal propagation in waveguides, the fundamental energy is confined into a few micrometers radius area over the complete crystal length. A 10% conversion efficiency is then attainable with less than 1 W of a c.w. pump power, which is about three orders of magnitude greater than in identical bulk materials. For example, a 3 mm long first-order QPM $LiNbO_3$ waveguide illuminated with 196 mW fundamental c.w. power generates 21 mW at the harmonic wavelength $\lambda = 426$ nm (28), which is very attractive for optical data storage applications for example.

The main limitations of the QPM devices come from the difficulties to realize large good-quality structures. The periodicity must be precisely preserved over the complete length of the sample, and the domain walls must be as small as possible to reduce the losses and achieve efficient conversion. The fabrication of bulk structures is even more complicated than for waveguides; the maximum thickness available at present is less than 1 mm. QPM applications then require strong focusing, and because of the optical damages, they are limited to low-power pump lasers.

Tuning of QPM can be achieved by thermalization or by an angular shift in the direction of propagation off the periodicity vector Λ of the structure. Angular, spectral, and thermal acceptance bandwidths are defined in much the same way for the case of birefringence phase-matching. For QPM, the angular noncritical situation corresponds to the normal to the structure which happens to be parallel to Λ. In that case, $\Delta\alpha$ is inversely proportional to the square root of the structure length L. α is the angle between the direction of propagation and the normal to the structure. Angular critical QPM corresponds to the normal to the device which makes a nonzero angle with Λ. $\Delta\alpha$ is then inversely proportional to L (5).

The critical and noncritical angular acceptance bandwidths for QPM are of the same order of magnitude as for birefringence phase-matching. An enhancement of these angular acceptances may be reached with different domain lengths and specially designed periodicity; even orders of the QPM can then be used. This optimization is detrimental to the conversion efficiency because the associated effective nonlinear coefficient is lowered.

Resonant SHG

SHG experiments with low-power pump lasers, especially c.w. lasers, yield to small single-pass conversion efficiencies. In that case, a net enhancement is obtained when the nonlinear material is placed inside a resonant cavity, and particularly directly inside the pump laser cavity, which is presented here. The corresponding devices are shown in Fig. 2(b, c). Actually, the transmission of the output mirror is generally low so that the fundamental intensity in the resonator is more important than the output intensity.

To achieve an intracavity device, the two cavity mirrors are total reflectors for the fundamental wave, and one of them, the output coupler, is perfectly transmitting at the harmonic wavelength. The coupling of the laser radiation is then made by the nonlinear medium, which is equivalent to a nonlinear transmission coefficient at ω equal to twice the single-pass SHG conversion efficiency.

The SHG intracavity device requires an intracavity polarizer. For type II phase-matching, it is useful to use a rotated quarter-waveplate in order to restitute the initial polarization of the fundamentals after a round trip in the nonlinear crystal, the retardation plate, and the mirror.

The intracavity SHG conversion efficiency is usually defined as the ratio of the generated harmonic power to the maximum fundamental power that would be delivered from the same laser without the nonlinear crystal but with optimum linear coupling (i.e., optimum transmission coefficient at ω for the output mirror) (29). This efficiency is severely reduced by all possible losses in the cavity. The absorption of the nonlinear crystal should then be as low as possible at both wavelengths. The crystal should be cut with high precision to allow the propagation along the chosen phase-matching direc-

tion in normal incidence; its surfaces should be well-polished and antireflection-coated to avoid scattering and undesirable reflection losses. Given these conditions, it is possible to achieve 100% conversion efficiencies. Based on the previous definition of the intracavity efficiency, the fundamental power is not completely converted into the harmonic inside the cavity in that case.

Such devices are used to generate very high harmonic powers. For example, 140 W average power at 0.532 μm is obtained with a 5 mm long KTP crystal placed in the cavity of a Q-switched Nd : YAG laser with a repetition rate of 25 kHz. External cavity SHG also leads to good results.

OPTICAL PARAMETRIC GENERATORS AND AMPLIFIERS

Second harmonic generators are particular cases of SFM optical parametric generators (OPG). In this section, we consider the general case where the parametric interaction can be an SFM or a DFM and where the two incident beams have different circular frequencies and different intensities. The incident waves are named the *pump wave* with the circular frequency ω_p and the *signal wave* at ω_s; the generated wave is the *idler wave* at ω_i with $\omega_i = \omega_p - \omega_s$. A schematic device is given in Fig. 10.

The nonlinear medium of the OPG or optical parametric amplifier (OPA) is not placed inside a resonant cavity. The device can have several functions, separated or not: the generation by SFM or DFM of a beam at ω_i for the OPG or the amplification by DFM of the beam at ω_s for the OPA. The device can exhibit the two functions for certain cases of DFM.

In order to simplify the integration of the system in Eq. (27), we consider that the waves are plane, and that the SFM and DFM are phase-matched in a direction of propagation without walk-off; furthermore, the pump is always undepleted, with or without depletion of the signal wave.

Pure Optical Parametric Generators

If the two incident beams are undepleted during the parametric interaction [i.e., $\partial E(\omega_p, Z)/\partial Z = \partial E(\omega_s, Z)/\partial Z \approx 0$], then, according to Eqs. (27), the intensities are

$$I(\omega_p, L) = T^2(\omega_p) I(\omega_p, 0) \tag{37}$$

$$I(\omega_s, L) = T^2(\omega_s) I(\omega_s, 0) \tag{38}$$

$$I(\omega_i, L) = \frac{\omega_i^2}{2}\left(\frac{\mu_0}{\epsilon_0}\right)^{3/2} \frac{(\epsilon_0 \chi_{\text{eff}})^2 T(\omega_p) T(\omega_s) T(\omega_i)}{n(\omega_p) n(\omega_s) n(\omega_i)} I(\omega_p, 0) I(\omega_s, 0) L^2 \tag{39}$$

with the parameters defined in Eq. (32).

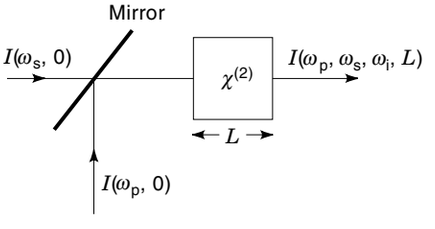

Figure 10. OPG or OPA device. $I(\omega_p, 0)$ and $I(\omega_s, 0)$ are the intensities of the incident beams. $I(\omega_p, L)$, $I(\omega_s, L)$, and $I(\omega_i, L)$ are the intensities at the exit of the nonlinear medium with the length L. $(\omega_i, \omega_s, \omega_p) = (\omega_1, \omega_2, \omega_3)$ with $\omega_3 = \omega_1 + \omega_2$.

The parametric interaction is an SFM when $(\omega_p, \omega_s, \omega_i) = (\omega_1, \omega_2, \omega_3)$ or $(\omega_2, \omega_1, \omega_3)$: the device is an up-conversion OPG because the generated circular frequency is bigger than the two incident ones. The process is a DFM when $(\omega_p, \omega_s, \omega_i) = (\omega_3, \omega_1, \omega_2)$ or $(\omega_3, \omega_2, \omega_1)$ or $(\omega_1, \omega_3, \omega_2)$ or $(\omega_2, \omega_3, \omega_1)$, and in that case we have a down-conversion OPG. The third harmonic generator is a widely used up-conversion OPG. In that case, $\omega_p = \omega$, $\omega_s = 2\omega$, and $\omega_i = 3\omega$. Such a device is based on the association of two nonlinear media, one for SHG ($\omega + \omega \rightarrow 2\omega$) and the other for THG ($\omega + 2\omega \rightarrow 3\omega$). A common example is the THG in KDP from a Nd : YAG laser emitting at 1.064 μm with a 10 Hz repetition rate and 8 ns pulse duration. For an incident energy equal to 600 mJ, it is typically possible to generate 300 mJ at 0.532 μm in the first KDP and 160 mJ at 0.355 μm in the THG KDP. In that case, Eqs. (37)–(39) are not valid because the two incident beams are depleted.

If only one incident beam is undepleted [i.e., $\partial E(\omega_p, Z)/\partial Z \approx 0$] and if ω_p is not the highest circular frequency (i.e., $\omega_p = \omega_1$ or ω_2), then, according to system (27), the intensities of the interacting beams are (30)

$$I(\omega_p, L) = T^2(\omega_p) I(\omega_p, 0) \tag{40}$$

$$I(\omega_s, L) = T^2(\omega_s) I(\omega_s, 0) \cos^2 \alpha L \tag{41}$$

$$I(\omega_i, L) = \frac{\omega_i}{\omega_s} T(\omega_s) T(\omega_i) I(\omega_s, 0) \sin^2 \alpha L \tag{42}$$

$$\text{with } \alpha = \epsilon_0 \chi_{\text{eff}} |E(\omega_p, 0)| \sqrt{T(\omega_p) \kappa_{\omega_s} \kappa_{\omega_i}} \tag{43}$$

where κ_{ω_s} and κ_{ω_i} are defined in the system in Eq. (25).

The parametric process is a DFM when $(\omega_i, \omega_s, \omega_p) = (\omega_2, \omega_3, \omega_1)$ or $(\omega_1, \omega_3, \omega_2)$ and a SFM when $(\omega_i, \omega_s, \omega_p) = (\omega_3, \omega_1, \omega_2)$ or $(\omega_3, \omega_2, \omega_1)$.

Because the functions in Eqs. (41) and (42) are periodic, the idler intensity $I(\omega_i)$ is maximum after the waves have propagated a distance $L_m = (2m + 1)\pi/2\alpha$ where m is an integer. At these points, the wave at ω_s is completely depleted and $I(\omega_i) = (\omega_i/\omega_s) T(\omega_s) T(\omega_i) I(\omega_s, 0)$. It is obvious that a nonlinear medium with a length $L_o = \pi/2\alpha$ is sufficient for an optimized device. L_o is typically equal to a few millimeters. Note that the maximum value of $I(\omega_i)$ is the same with or without the depletion of the pump beam.

In Fig. 11 are plotted the pure OPG Eqs. (37)–(43).

Mixed Optical Parametric Generators and Amplifiers

If the beam at the highest frequency is the only one to be undepleted [i.e., $\partial E(\omega_p = \omega_3, Z)/\partial Z \approx 0$], the different intensities are expressed as (30)

$$I(\omega_p = \omega_3, L) = T^2(\omega_3) I(\omega_3, 0) \tag{44}$$

$$I(\omega_s, L) = T^2(\omega_s) I(\omega_s, 0) \operatorname{ch}^2 \beta L \tag{45}$$

$$I(\omega_i, L) = \frac{\omega_i}{\omega_s} T(\omega_s) T(\omega_i) I(\omega_s, 0) \operatorname{sh}^2 \beta L \tag{46}$$

$$\text{with } \beta = \epsilon_0 \chi_{\text{eff}} |E(\omega_p, 0)| \sqrt{T(\omega_3) \kappa_{\omega_1} \kappa_{\omega_2}} \tag{47}$$

The parametric interaction is a DFM, with $(\omega_i, \omega_s) = (\omega_1, \omega_2)$ or (ω_2, ω_1).

Equations (45) and (46), which are plotted on Fig. 12, show that the generation of the idler wave is not obtained to the

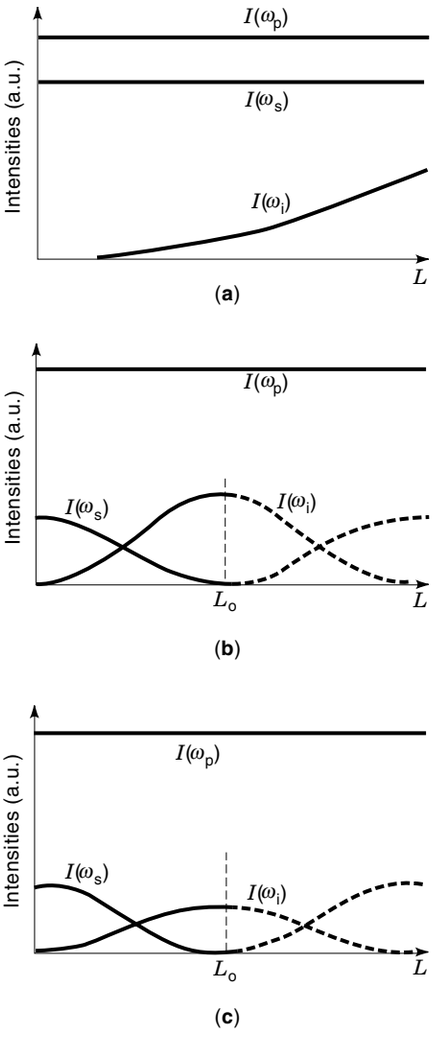

Figure 11. Pure OPG intensity behaviors. (a) Two undepleted beams: SFM with $(\omega_i, \omega_s, \omega_p) = (\omega_3, \omega_1, \omega_2)$ or $(\omega_3, \omega_2, \omega_1)$ and DFM with $(\omega_i, \omega_s, \omega_p) = (\omega_2, \omega_1, \omega_3)$ or $(\omega_1, \omega_2, \omega_3)$ or $(\omega_2, \omega_3, \omega_1)$ or $(\omega_1, \omega_3, \omega_2)$. (b) One undepleted beam: SFM with $(\omega_i, \omega_s, \omega_p) = (\omega_3, \omega_1, \omega_2)$ or $(\omega_3, \omega_2, \omega_1)$. (c) One undepleted beam: DFM with $(\omega_i, \omega_s, \omega_p) = (\omega_2, \omega_3, \omega_1)$ or $(\omega_1, \omega_3, \omega_2)$.

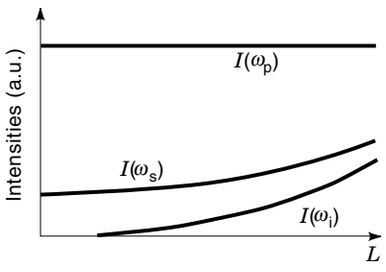

Figure 12. Mixed OPG-OPA intensity behaviors. DFM with $(\omega_i, \omega_s, \omega_p) = (\omega_1, \omega_2, \omega_3)$ or $(\omega_2, \omega_1, \omega_3)$.

detriment of the signal wave, which is contrary to the pure OPG with one undepleted beam. Consequently, such a device also has the function of an OPA.

The gain of the OPA can be defined as

$$G(L) = \left| \frac{I_s(L)}{I_s(0)} - 1 \right| \tag{48}$$

We take the example of the parametric amplification of a beam at 0.355 μm by a pump at 1.064 μm. A gain of about 10 can be obtained at the exit of a 5 cm long KD_2PO_4 crystal with a pump intensity of 28 MW/cm^2 (30).

Then the mixed OPG-OPA is of great interest when it is difficult to measure a weak signal in the infrared range, at $\omega_s = \omega_1$, where the usual detectors have a small detectivity. Indeed, this device makes it possible to amplify the signal (OPA function), which can help for the detection at its own circular frequency; the other issue is to get the information concerning ω_1 by the measurement of the generated idler frequency (OPG function), at $\omega_i = \omega_2 > \omega_1$, when the pump beam at $\omega_p = \omega_3$ is properly chosen (e.g., in the visible range, such as ω_2 is in the near infrared where the detection is easy). Note that a pure SFM OPG can also be used for up-conversion: the signal at $\omega_s = \omega_1$ is mixed with the pump at $\omega_p = \omega_2$ for the generation of the idler circular frequency $\omega_i = \omega_3$, which will be measured; according to Eq. (42) the maximum intensity that can be generated at ω_3 is unfortunately limited by the weak signal intensity [i.e., $I_{max}(\omega_3) = I(\omega_3, L_o) = (\omega_3/\omega_1)T(\omega_3)T(\omega_1)I(\omega_1, 0)$]. Then, if $I(\omega_3, L_o)$ has not a sufficient level for a good detection, it is necessary to realize the up-conversion with a mixed OPG-OPA as already described: the generated idler circular frequency $\omega_i = \omega_3 - \omega_1 = \omega_2$ is lower than in the case of the SFM OPG (i.e., $\omega_i = \omega_1 + \omega_2 = \omega_3$). On the other hand, the maximum intensity that it is possible to generate is not limited by the weak signal but by the strong pump [i.e., $I_{max}(\omega_2) = (\omega_2/\omega_3)T(\omega_3)T(\omega_2)I(\omega_3, 0)$]. This value is reached when the pump at ω_3 is completely depleted; then Eq. (46) is not valid, and the calculation of $I_{max}(\omega_2)$ can be done by considering the exact solution of the system in Eq. (27) (i.e., the Jacobian elliptic functions, or more simply by using Manley–Rowe relations).

OPTICAL PARAMETRIC OSCILLATORS

When a strong laser beam at ω_p propagates in a $\chi^{(2)}$ medium, there exists a probability that these photons spontaneously break down into a continuous range of pairs of lower-energy photons of circular frequencies ω_s and ω_i with the total photon energy conserved for each of the pairs (i.e., $\omega_s + \omega_i = \omega_p$). This phenomenon is called *spontaneous parametric emission* or *parametric noise* (31).

The amplification of the corresponding generated waves is possible during their propagation in the nonlinear medium by the process of OPA described in the previous section. The pairs of generated waves for which the phase-matching condition is satisfied [i.e., $\boldsymbol{k}(\omega_s) + \boldsymbol{k}(\omega_i) = \boldsymbol{k}(\omega_p)$] are the only ones to be efficiently amplified.

The intensities generated after a single pass in the nonlinear medium are small because of the weak parametric noise intensity, even in a phase-matching direction. The parametric amplification is a stimulation emission process, so its effi-

ciency depends on the intensity of the interacting waves, according to system (27). Consequently, the efficiency of the OPA can be enhanced if the nonlinear medium is placed inside a resonant cavity that constitutes an optical parametric oscillator (OPO) (32). The OPO can be singly resonant (SROPO) at ω_s or ω_i, doubly resonant (DROPO) at both ω_s and ω_i, or triply resonant (TROPO), at ω_s, ω_i, and ω_p. The oscillation of the chosen generated waves begins when the parametric gain, which depends on the pump intensity, is sufficiently high to compensate the cavity losses. For that, it is necessary to pump the OPO above a minimum intensity level, which is termed as threshold pump intensity I_{th}. The losses are essentially the linear absorption in the nonlinear medium and the transmission coefficient of the output coupler mirror.

I_{th} decreases when the number of resonant frequencies increases. On the other hand, the instability increases because the condition of simultaneous resonance is critical.

The threshold pump intensity of a SROPO or a DROPO can be reduced by reflecting the pump from the output coupler mirror. For a SROPO at ω_s and for a pulsed pump beam with an intensity that is supposed to be constant over a single-pass, I_{th} is given by (33)

$$I_{th} = \frac{1.8}{\kappa_s L^2 (1+\gamma)^2}\left[\frac{25L}{c\tau} + 2\alpha L + \ln\left(\frac{1}{\sqrt{1-T(\omega_s)}}\right) + \ln(2)\right]^2 \tag{49}$$

$\kappa_s = \omega_s \omega_i \chi^2_{eff}/[2n(\omega_s)n(\omega_i)n(\omega_p)\epsilon_0 c^3]$, L is the length of the nonlinear medium, $\gamma \approx 1$ is the ratio of the backward to the forward pump intensity, τ is the $1/e^2$ half width duration of the pump beam intensity, (2α) is the linear absorption coefficient, and $T(\omega_s)$ is the transmission coefficient of the output coupler at ω_s.

Equation (49) shows that as the losses increase, the effective coefficient must also increase in order to work at a lower threshold pump intensity. In the nanosecond regime, which is the case of the most part of the currently commercially available OPOs, the typical values of I_{th} are in the range 10–100 MW/cm^2.

There exist two main techniques for the OPO pump injection, as shown in Fig. 13. In Fig. 13(a), the pump beam propagates in the axis of the cavity. For continuous waves or pulsed waves with pulse durations greater than 1 ns, it is possible to increase the cavity length in order to place inside the cavity two 45° mirrors that reflect the pump beam. It corresponds to Fig. 13(b), which allows us to protect the cavity mirrors and to use for them simpler dielectric coatings.

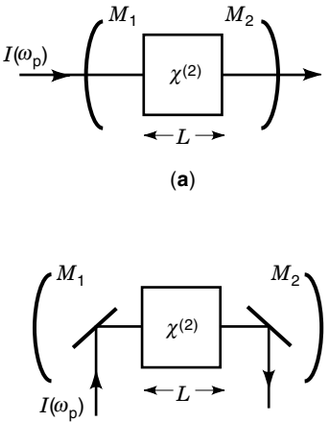

Figure 13. Configurations of OPO pump injection. (a) An SROPO, an DROPO, or an TROPO according to the reflectivity of mirrors M_1 and M_2. (b) An SROPO or a DROPO.

In any case, it is necessary to pump an OPO by a beam with a smooth optical profile because hot spots could damage all the optical components in the OPO: mirrors and nonlinear crystal. Furthermore, an OPO requires a pump beam of very high quality with regard to other parameters such as the spectral bandwidth, the pointing stability, the divergence, and the pulse duration; their respective role are discussed later according to the specificity of the device.

OPOs can be used to generate a fixed wavelength, idler, or signal, but their real interest is in the wavelength tunability over a broad range, from the near ultraviolet to the mid infrared. As we saw previously, the range of pairs (ω_s, ω_i) that can be amplified depends on the spectral range of phase-matching and then on the refractive indices. The tuning is based on the dispersion of the refractive indices with the wavelength, the direction of propagation, the temperature, or any other variable of dispersion. The choice of the nonlinear medium is then of prime importance because phase-matching must exist over the widest spectral range for a reasonable variation of the considered dispersion parameter. Several methods are used: rotation of the nonlinear crystal, variation of pump wavelength, modification of the temperature, or application of a static or low-frequency electric field. Angle tuning and pump wavelength tuning are the most frequently used methods at present for birefringence phase-matching.

Optical Parametric Oscillators at Fixed Wavelengths

The pump wavelength is fixed, and the nonlinear crystal is cut so that the phase-matching direction of the considered interaction is collinear to the cavity axis. The output coupler M_2 can be transparent at ω_s or ω_i or at both circular frequencies, according to the application. The prototypical single-frequency OPO is an SROPO that emits an eye-safe wavelength at 1.61 μm (34). The OPO is pumped at 1.064 μm by a Q-switched Nd:YAG laser with a $1/e^2$ pulse duration of 15 ns. The pump coupling is coaxial as in Fig. 13(a): the pump coupler M_1 has high reflection at 1.61 μm and high transmission at 1.064 μm, and the output coupler M_2 has high reflection at 1.064 μm and a 10% transmission coefficient at 1.61 μm. The nonlinear medium is an x-cut 20 mm long KTP crystal: the principal x-axis is a type II phase-matching direction for the DFM 1/1.064 μm − 1/3.14 μm = 1/1.61 μm; it is an angular NCPM direction. An energy of 9 mJ at 1.61 μm is obtained from 20 mJ at 1.064 μm corresponding to an intensity of 160 MW/cm^2. This device is currently used for telemetry.

Optical Parametric Oscillators with Angle Tuning

The function of these devices is to generate the signal and idler waves over a broad range, $\Delta\omega_s$ and $\Delta\omega_i$, respectively, from a fixed pump wave at ω_p (35). The spectral shifts $\Delta\omega_s = \omega_s^+ - \omega_s^-$ and $\Delta\omega_i = \omega_i^+ - \omega_i^-$ are obtained by rotating the nonlinear crystal by an angle $\Delta\alpha = \alpha^+ - \alpha^-$ in order to achieve successively phase-matching over the considered spectral range [i.e., $\omega_p\, n(\omega_p, \alpha) = \omega_s\, n(\omega_s, \alpha) + \omega_i\, n(\omega_i, \alpha)$, from $(\omega_i^-, \omega_s^-, \alpha^-)$ to $(\omega_i^+, \omega_s^+, \alpha^+)$]. We give the example of the phase-

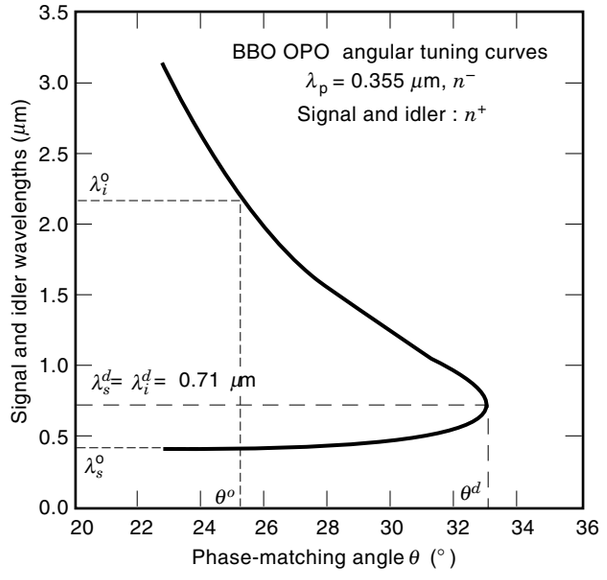

(**a**)

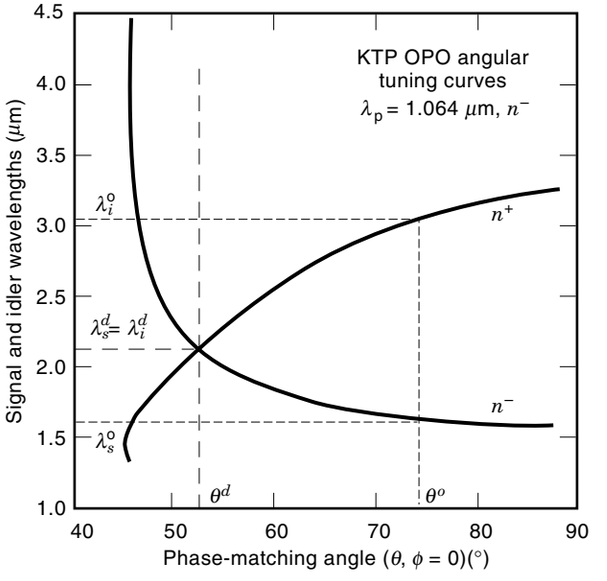

(**b**)

Figure 14. OPO angular tuning curves of (a) BBO and (b) KTP. θ is the internal phase-matching angle.

matching tuning curves $\lambda_i(\alpha)$ and $\lambda_s(\alpha)$ for BBO and KTP, which are widely used in broadband devices. The curves of Fig. 14 are calculated with the relation in Eq. (19) for BBO and relations (20) and (21) for KTP.

The nonlinear crystal and the phase-matching directions are chosen so that the tuning rate $\Delta\omega_{i,s}/\Delta\alpha$ is maximum because $\Delta\alpha$ cannot exceed about 30° of arc (i.e., 15° on either side of the direction normal to the surface of the nonlinear crystal). Actually the refraction can lead to an attenuation of the efficiency of the parametric interaction for bigger angles. For this reason, the broadband device necessarily requires a nonlinear crystal with angular CPM (i.e., $\partial\lambda_{i,s}/\partial\alpha \neq 0$), over a broad spectral range.

The angular criticality of the phase-matching is detrimental to the wavelength stability of the signal and idler waves with respect to the pointing fluctuation of the pump beam. A pointing stability on the order of 100 μrad is considered to be acceptable with crystals such as KTP and BBO. Because of the angular criticality, the spectral bandwidth of the generated beams, $\delta\omega_i$ and $\delta\omega_i$, strongly depends on the divergence of the pump beam. A larger value of $\partial\lambda_{i,s}/\partial\alpha$ corresponds to higher spectral bandwidths for a given pump divergence. Furthermore, the derivative varies according to the phase-matching direction as it is shown in Fig. 14. $\partial\lambda_{i,s}/\partial\alpha$ is maximum at the degeneracy for type I (i.e., for $\lambda_i = \lambda_s$), and at the short angle cutoff of the phase-matching curve for type II. That implies that the spectral bandwidth of the signal and idler waves can vary considerably over the considered spectral range, especially for type I: a variation from 500 to 50 cm^{-1} is common along a typical type I phase-matching curve; the spectral bandwidth (expressed in cm^{-1}) is defined as $\delta\lambda_{i,s}/\lambda_{i,s}^2$.

These broad spectral bandwidths are too large for a few applications such as spectroscopy. A weak reduction can be achieved by using an injection seeded pump. Indeed, the phase-matching is λ-noncritical according to its angular criticality. On the other hand, the use of a single-mode pump allows a better stability of the idler and signal intensities. The only way to substantially reduce the spectral bandwidth is to introduce bandwidth-limiting elements in the OPO cavity (e.g., a grazing grating associated with a tuning mirror reflecting either the signal or the idler according to the chosen resonance). The rotations of the nonlinear crystal and of the restricting elements must be synchronized in order to be active over the generated wavelength range. Narrow bandwidths of about 0.1 cm^{-1} can be obtained, but unfortunately the gain of such devices is low. Nevertheless, high energy and narrow bandwidth can both be obtained by the association of a narrow band OPO with a mixed OPA–OPG, which is also pumped at ω_p. The seed wave emitted by the narrow band OPO (i.e., either the signal or the idler) is amplified, and the other one is generated, as explained in the previous section. The OPA can be placed inside a resonant cavity in order to increase the gain.

Optical Parametric Oscillators with Pump Tuning

The nonlinear crystal is fixed, and the pump circular frequency can vary over $\Delta\omega_p$ leading to a variation of the signal and idler frequencies $\Delta\omega_s$ and $\Delta\omega_i$, respectively. For a given pump wavelength range $\Delta\omega_p$, the nonlinear crystal and the phase-matching direction are chosen in order to get the highest tuning rate $\Delta\omega_{i,s}/\Delta\omega_p$. The most favorable situation is obviously an angular NCPM direction because it is a wavelength critical direction. Figure 15 shows that RTA is suitable for an OPO pumped by a Ti : Sapphire laser (36).

Because of angular NCPM, the OPO with pump tuning has a low sensitivity to the divergence and pointing fluctuation of the pump beam, as opposed to an angular CPM OPO. Furthermore, the walk-off angle is nil, allowing us to use a longer nonlinear crystal and then to provide a higher conversion efficiency.

Multigrating Quasi-PhaseMatched OPO

In a QPM device, the interacting frequencies are fixed by the frequency dispersion of the birefringence of the nonlinear ma-

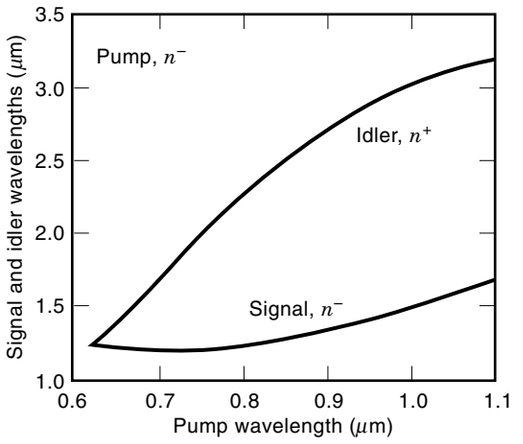

Figure 15. Phase-matching tuning curve of RTA for type II SFM.

terial and by the periodicity of the grating. A series of gratings with different periodicities are fabricated in the same nonlinear crystal; the translation of this crystal with respect to the fixed pump beam allows us to address the different gratings and then to generate different couples (ω_s, ω_i). Because the tuning is obtained in discrete steps, it is necessary to combine temperature or angle tuning with the translation of the sample in order to make a smooth interpolation between the steps. This device has been recently developed with a periodically poled $LiNbO_3$ (PPLN) with a thickness of 0.5 mm and a length along the periodicity vector of 1 cm (37). A total of 25 gratings with periods between 26 and 32 μm are realized in 0.25 μm increments. The OPO is pumped at 1.064 μm and generates a signal between 1.35 and 1.98 μm, and the corresponding idler generates a signal between 4.83 and 2.30 μm.

RECENT ADVANCES IN FREQUENCY CONVERSION

Many applications require solid-state laser sources, with a wider spectral range, better tuning capabilities, higher output energies, and optimum beam quality. Apart for the amelioration of the pump lasers performances, the corresponding optimization of the frequency converters mainly concerns two aspects: the nonlinear medium and the device itself. The previous parts of the text and the examples given therein present some of the advanced fields in optical frequency conversion. Resonant devices and walk-off compensation are attractive ways to enhance conversion efficiencies. A particular effort is made to obtain large QPM structures with good optical quality. The reader interested in advances concerning parametric devices may refer to Refs. (38) and (39).

The research of new nonlinear materials deals with:

- enlarged transparency ranges toward the ultraviolet (e.g., for photolithography applications) and toward the infrared (e.g., for spectroscopy applications)
- higher nonlinear dielectric susceptibilities
- extended phase-matching tuning ranges, especially with the existence of noncritical phase-matching for interactions of particular interest
- increased damage threshold

In order to allow the development of commercial devices, these materials must also have good mechanical and chemical stability. New materials are searched among the inorganic and organic compounds, and more recently mixed organic-inorganic components were developed. An important field of research also concerns quantum wells, fibers, thin films, and polymers that can exhibit interesting nonlinear properties.

The study of any new material generally requires important material processing efforts, and the sample sizes are generally small at such early stages. Development of performant methods for the characterization of linear and nonlinear optical properties is then of prime importance (40).

Concerning the devices, efforts are being made on nanosecond systems, which constitute powerful sources, as developed in this article. Note that special effort has been made on short pulse devices, because of their high potentialities for telecommunication systems, all the more so since optical fibers are progressing at the same time. Once again, the reader interested in those particular aspects should refer to specialized texts.

New devices have been developed to achieve several interactions simultaneously. One particular example is called *tandem OPO.* Two crystal are placed in the resonant cavity. The first one generates signal and idler waves ω_{s_a} and ω_{i_a} from the incoming pump at ω_p; the second crystal is chosen to allow phase-matching with the previous signal ω_{s_a} acting as a pump and generates ω_{s_b} and ω_{i_b} such as $\omega_{s_a} = \omega_{s_b} + \omega_{i_b}$ (41). These devices allow us to generate two more wavelengths from the unique pump and to possibly extend the tuning range. Similar devices associate one OPO and one SFM in the same cavity, or one OPO and one SHG, or one OPO and one DFM. It is worth noting that for very particular combinations of wavelengths, the two interactions may be phase-matched along the same direction, and one unique crystal is then used.

Another advance in the field of OPOs may come from intracavity OPOs: they take advantage of the more important pump intensity inside the laser cavity, and should then allow high conversion efficiencies (42).

All these devices involve an additional coupling, and their overall behavior is more complicated than the single-crystal devices.

BIBLIOGRAPHY

1. N. Bloembergen, *Nonlinear Optics,* New York: Benjamin, 1965.
2. P. N. Butcher and D. Cotter, *The Elements of Nonlinear Optics,* Cambridge Series in Modern Optics, Cambridge: Cambridge University Press, 1991.
3. B. Boulanger and G. Marnier, Field factor calculation for the study of the relationships between all the 3-wave nonlinear optical interactions in uniaxial and biaxial crystals, *J. Phys. Condens. Matter,* **3**: 8327–8350, 1991.
4. J. F. Nye, *Physical Properties of Crystals,* Oxford: Clarendon Press, 1957.
5. M. M. Fejer et al., Quasi-phase-matched second harmonic generation: Tuning and tolerances, *IEEE J. Quantum Electron.,* **QE-28**: 2631–2653, 1992.
6. J. P. Feve, B. Boulanger, and G. Marnier, Calculation and classification of the direction loci for collinear types I, II and III phase-matching of three-wave nonlinear optical parametric interactions in uniaxial and biaxial acentric crystals, *Optics Comm.,* **99**: 284–302, 1993.

7. P. F. Bordui and M. M. Fejer, Inorganic crystals for nonlinear optical frequency conversion, *Annu. Rev. Mater. Sci.,* **23**: 321–379, 1993.
8. D. S. Chemla and J. Zyss (eds.), *Nonlinear Optical Properties of Organic Molecules and Crystals,* New York: Academic Press, 1987.
9. Y. R. Shen, *The Principles of Nonlinear Optics,* New York: Wiley, 1984.
10. V. G. Dmitriev, G. G. Gurzadyan, and D. N. Nikogosyan, *Handbook of Nonlinear Optical Crystals,* Berlin-Heidelberg: Springer Verlag, 1991.
11. D. Eimerl, High average power harmonic generation, *IEEE J. Quantum Electron.,* **QE-23**: 575–592, 1987.
12. P. Pliszka and P. Banerjee, Nonlinear transverse effects in second-harmonic generation, *J. Opt. Soc. Amer. B,* **10** (10): 1810–1819, 1993.
13. A. V. Smith et al., Comparison of a numerical model with measured performance of a seeded, nanosecond KTP optical parametric oscillator, *J. Opt. Soc. Amer. B,* **12** (11): 2253–2267, 1995.
14. T. Nishikawa and N. Uesugi, Effects of walk-off and group velocity difference on the optical parametric generation in $KTiOPO_4$ crystals, *J. Appl. Phys.,* **77** (10): 4941–4947, 1995.
15. G. E. Francois, c.w. measurement of the optical nonlinearity of ammonium dihydrogen phosphate, *Phys. Rev.,* **143** (2): 597–600, 1966.
16. M. V. Hobden, Phase-matched second harmonic generation in biaxial crystals, *J. Appl. Phys.,* **38** (11): 4365–4372, 1967.
17. S. X. Dou et al., Comparison between collinear and noncollinear phase matching for second-harmonic and sum-frequency generation in 3-methyl-4-nitropyridine-1-oxide, *J. Opt. Soc. Amer. B,* **9** (5): 687–697, 1992.
18. S. G. Dolinchuk, N. E. Kornienko, and V. I. Zadorozhnii, Noncritical vectorial phase matchings in nonlinear optics of crystals and infrared up-conversion, *Infrared Phys. Technol.,* **35** (7): 881–895, 1994.
19. G. D. Boyd et al., Second-harmonic generation of light with double refraction, *Phys. Rev.,* **137** (4A): 1305, 1965.
20. S. C. Mehendale and P. K. Gupta, Effect of double refraction on type II phase-matched second harmonic generation, *Optics Comm.,* **68** (4): 301–304, 1988.
21. J. J. Zondy, Comparative theory of walk-off limited type II versus type I second harmonic generation with gaussian beams, *Optics Comm.,* **81** (6): 427–440, 1991.
22. S. X. Dou, D. Josse, and J. Zyss, Noncritical properties of noncollinear phase-matched second-harmonic and sum-frequency generation in 3-methyl-4-nitropyridine-1-oxide, *J. Opt. Soc. Amer. B,* **8** (8): 1732–1739, 1991.
23. J. J. Zondy et al., Walkoff-compensated type-I and type-II SHG using twin-crystal $AgGaSe_2$ and $KTiOPO_4$ devices, *Proc. SPIE,* **2700**: 66–72, 1996.
24. A. J. W. Brown et al., High-energy, high-efficiency second-harmonic generation of 1064-nm radiation in KTP, *Opt. Lett.,* **17** (2): 109–111, 1992.
25. S. P. Velsko et al., >100 watt average power at 0.53 μm with 25 ns, 2.5 kHz repetition rate pulses from a single power oscillator, *Proc. SPIE,* **2206**: 484–488, 1993.
26. R. C. Eckardt and J. Reintjes, Phase matching limitations of high efficiency second harmonic generation, *IEEE J. Quantum Electron.,* **QE-20** (10): 1178–1187, 1984.
27. J. P. Meyn and M. M. Fejer, Tunable ultraviolet radiation by second harmonic generation in periodically poled lithium tantalate, *Opt. Lett.,* **22** (16): 1214–1216, 1997.
28. M. Yamada et al., First-order quasi-phase matched $LiNbO_3$ waveguide periodically poled by applying an external field for efficient blue second-harmonic generation, *Appl. Phys. Lett.,* **62** (5): 435–436, 1993.
29. R. G. Smith, Theory of intracavity optical second harmonic generation, *IEEE J. Quantum Electron.,* **QE-6** (4): 215–223, 1970.
30. R. A. Baumgartner and R. L. Byer, *IEEE J. Quantum Electron.,* **QE-15** (6): 432, 1979.
31. W. H. Louisell, A. Yariv, and A. E. Siegman, *Phys. Rev.,* **124**: 1646, 1961.
32. R. L. Byer, Optical parametric oscillators, in H. Rabin and C. L. Tang (eds.), *Treatise in Quantum Electronics,* New York: Academic Press, 1973.
33. S. J. Brosnan and R. L. Byer, Optical parametric oscillator threshold and linewidth studies, *IEEE J. Quantum Electron.,* **QE-15** (6): 415–431, 1979.
34. L. R. Marshall and A. Kaz, Eye-safe output from noncritically phase-matched parametric oscillators, *J. Opt. Soc. Amer. B,* **10** (9): 1730–1736, 1993.
35. C. L. Tang et al., Optical parametric oscillators, *Proc. IEEE,* **80**: 365–373, 1992.
36. D. T. Reid, M. Ebrahimzadeh, and W. Sibbett, Noncritically phase-matched Ti : sapphire-pumped femtosecond optical parametric oscillator based on $RbTiOAsO_4$, *Opt. Lett.,* **20** (1): 55–57, 1995.
37. L. E. Myers et al., Multigrating quasi-phase-matched optical parametric oscillator in periodically poled $LiNbO_3$, *Opt. Lett.,* **21** (8): 591–593, 1996.
38. Special issue on optical parametric oscillation and amplification, *J. Opt. Soc. Amer. B,* **10**: 1659–2239, 1993.
39. Special issue on optical parametric devices, *J. Opt. Soc. Amer. B,* **12**: 2087–2322, 1995.
40. B. Boulanger et al., Absolute measurement of quadratic nonlinearities from phase-matched second-harmonic generation in a single KTP crystal cut as a sphere, *J. Opt. Soc. Amer. B,* **14** (6): 1380–1386, 1997.
41. G. T. Moore and K. Koch, The tandem optical parametric oscillator, *IEEE J. Quantum Electron.,* **32**: 2085–2094, 1996.
42. T. Debuisschert et al., Intracavity optical parametric oscillator: Study of the dynamics in pulsed regime, *J. Opt. Soc. Amer. B,* **13** (7): 1569–1587, 1996.

B. BOULANGER
J. P. FÈVE
Laboratoire de Physique de
l'Université de Bourgogne

OPTICAL INSTRUMENTS. See INTERFEROMETERS.

OPTICAL INTERCONNECTS. See SYSTEM INTERCONNECTS.

OPTICAL ISOLATORS. See FARADAY EFFECT.

OPTICAL LITHOGRAPHY. See PHOTOLITHOGRAPHY.